Disorder-free Sachdev-Ye-Kitaev models: Integrability and a precursor of chaos

Soshun Ozaki [1] and Hosho Katsura [2,3,4]

[1] *Department of Basic Science, The University of Tokyo, Komaba, Meguro-ku, Tokyo 153-0041, Japan*
[2] *Department of Physics, The University of Tokyo, Hongo, Bunkyo-ku, Tokyo 113-0033, Japan*
[3] *Institute for Physics of Intelligence, The University of Tokyo, Hongo, Bunkyo-ku, Tokyo 113-0033, Japan*
[4] *Trans-scale Quantum Science Institute, The University of Tokyo, Hongo, Bunkyo-ku, Tokyo 113-0033, Japan*

(Received 11 July 2024; accepted 3 January 2025; published 23 January 2025)

We introduce two disorder-free variants of the Sachdev-Ye-Kitaev (SYK) model, demonstrate their integrability, and study their static and dynamical properties. Unlike diagrammatic techniques, the integrability of these models allows us to obtain dynamical correlation functions even when the number of Majorana fermions is finite. From the solutions, we find that out-of-time-order correlators (OTOCs) in these models exhibit exponential growth at early times, resembling that of many-body quantum chaotic systems, such as those with disorder or external kick terms, despite their large N behavior differing from that of typical chaotic systems. Conversely, our analysis shows no evidence of random-matrix behavior in level spacing statistics or the spectral form factor. Our findings illustrate that the clean versions of the SYK models represent simple but nontrivial examples of disorder-free quantum many-body systems displaying chaoslike behavior of OTOCs.

DOI: 10.1103/PhysRevResearch.7.013092

I. INTRODUCTION

The nonequilibrium dynamics of quantum many-body systems is one of the central issues in modern physics, encompassing concepts such as thermalization [1–3], many-body quantum chaos [4–6], quantum scars [7–9], and many-body localization [10–12]. Recently, there has been renewed interest in many-body quantum chaos, not only within statistical physics but also in high-energy physics and quantum information theory. This resurgence is motivated by the conjecture that black holes act as fast scramblers [13–17] and the proposal of the Sachdev-Ye-Kitaev (SYK) model [18–22]. To date, various metrics have been proposed for diagnosing quantum chaos [23].

Commonly used criteria in analyzing quantum chaotic systems include level spacing statistics and the spectral form factor (SFF). These criteria are based on the conjecture that such systems exhibit properties akin to those of random matrices. Specifically, the level spacing statistics of quantum chaotic systems are expected to follow the Wigner-Dyson distribution, as exemplified in Refs. [24,25]. Additionally, the SFF, interpreted as the two-point correlation function of energy levels, is believed to capture the features of quantum chaos [26,27].

In recent years, the out-of-time-order correlators (OTOCs) [28–31] have emerged as another significant indicator of quantum chaos. OTOCs are defined using the quantum counterpart of Poisson brackets in classical mechanics. As in some one-body chaotic systems with periodic kicking, OTOCs in quantum many-body chaotic systems are believed to exhibit scrambling, i.e., exponential growth at early times followed by rapid decay to zero. This behavior is commonly observed in quantum many-body systems with disorder or periodic driving. In particular, the exponential growth of OTOCs at early times corresponds to the sensitivity to initial conditions inherent in classical chaotic systems. This exponential growth is quantified by the quantum Lyapunov exponent λ [14,17], which has been conjectured to be bounded as $\lambda \leqslant 2\pi T$ where T is the temperature. This upper bound is referred to as the Maldacena-Shenker-Stanford (MSS) bound. It has been confirmed that some models considered chaotic exhibit this exponential growth in OTOCs [32,33]. Note, however, that the OTOC is not a definitive indicator of chaos [31,34–36], nor is the SFF [26]. In this paper we say that a quantum many-body system is chaotic if it exhibits Wigner-Dyson-type level spacing statistics, random matrixlike SFF, and the scrambling of OTOCs.

These indicators are effective when applied to the SYK model; Level spacing statistics and SFF exhibit random matrixlike behavior [37–40], while the OTOC shows exponential growth [19,29,30,41]. In this paper, we show that the OTOC can also detect anomalous dynamics occurring in the disorder-free variants of the SYK model [42], which we dub the clean SYK models. These models are integrable in the sense that their energy eigenvalues and eigenstates can be obtained explicitly. After demonstrating the integrability, we investigate the OTOC, level spacing statistics, and SFF using the obtained solutions. We find that the OTOC shows an exponential growth at early times despite the integrability of the models, although the duration is much shorter than that of the typical chaotic systems. This behavior may be interpreted as a precursor of chaos. In contrast, we observe that the level

Published by the American Physical Society under the terms of the Creative Commons Attribution 4.0 International license. Further distribution of this work must maintain attribution to the author(s) and the published article's title, journal citation, and DOI.

spacing statistics and SFF of the models do not exhibit random matrixlike behavior. Studying the chaos-reminiscent behavior of the OTOC, which is analytically tractable even for finite N, may enhance our understanding of the chaotic dynamics of the (original) SYK model.

This paper is organized as follows. In Sec. II, we introduce two disorder-free variants of the SYK model and demonstrate their integrability by finding their analytical solutions explicitly. In Sec. III, we numerically study the many-body density of states and level-spacing statistics of these models. In Sec. IV, we investigate the fundamental thermodynamic properties and discuss the residual entropy. In Sec. V, we examine dynamical properties. We formulate two-point functions and OTOCs and evaluate them numerically. Furthermore, we discuss the exponential behaviors of OTOCs. In Sec. VI, we numerically evaluate SFF and verify the scaling law obtained from analytical approximation. Finally, we present a summary in Sec. VII.

II. MODELS AND SOLUTIONS

We start with a simple variant of the SYK model with uniform coupling [43]

$$H_4 = \mathrm{i}^2 \sum_{1\leqslant i_1<i_2<i_3<i_4\leqslant N} \gamma_{i_1}\gamma_{i_2}\gamma_{i_3}\gamma_{i_4}, \tag{1}$$

where γ_i $(i = 1, \ldots, N)$ are Majorana fermions satisfying $\gamma_i^\dagger = \gamma_i$ and $\{\gamma_{i_1}, \gamma_{i_2}\} = 2\delta_{i_1 i_2}$. To solve H_4, we introduce the auxiliary quadratic Hamiltonian

$$H_2 = \mathrm{i} \sum_{1\leqslant i_1<i_2\leqslant N} \gamma_{i_1}\gamma_{i_2}. \tag{2}$$

A straightforward calculation shows that this Hamiltonian and H_4 are related to each other via

$$H_4 = \frac{1}{2}(H_2)^2 + E_0, \quad E_0 = -\frac{N(N-1)}{4}. \tag{3}$$

The derivation of Eq. (3) is provided in Appendix A 1. Consequently, diagonalization of H_4 is reduced to that of H_2.

To diagonalize H_2, we define the creation and annihilation operators for fermions by the Fourier transform of the Majorana operators:

$$f_k^\pm = \frac{1}{\sqrt{2N}} \sum_{j=1}^{N} e^{\mp \mathrm{i}(j-1)\theta_k}\gamma_j, \tag{4}$$

where $\theta_k = (2k-1)\pi/N$ $(k = 1, \ldots, \frac{N}{2})$, and $f_k^\pm$ satisfy the anticommutation relations: $\{f_k^s, f_{k'}^{\bar{s}'}\} = \delta_{ss'}\delta_{kk'}$ with $\bar{s}'(s' = +, -)$ being a short-hand notation for $-s'$. Then, we can rewrite H_2 as

$$H_2 = \sum_{k=1}^{\frac{N}{2}} \epsilon_k \left(n_k - \frac{1}{2}\right), \quad \epsilon_k = 2\cot\frac{\theta_k}{2}, \tag{5}$$

where $n_k = f_k^+ f_k^-$ are the number operators for fermions, each of which takes the values 0 or 1. In this fermionic representation, the number of k's is $N/2$, which is consistent with the fact that the number of Majorana fermions is N, since the degrees of freedom of Majorana fermions are half of those of complex fermions. Equation (5) indicates that H_2 is diagonal in the fermion number basis, and therefore H_4 is. The energy eigenvalues of H_2 and H_4 specified by the occupation numbers $n_1, \ldots, n_{\frac{N}{2}}$ are

$$E_2\left(n_1, \ldots, n_{\frac{N}{2}}\right) = \frac{1}{2}\sum_{k=1}^{\frac{N}{2}} (-1)^{n_k+1}\epsilon_k, \tag{6}$$

and

$$E_4\left(n_1, \ldots, n_{\frac{N}{2}}\right) = \tfrac{1}{2}E_2\left(n_1, \ldots, n_{\frac{N}{2}}\right)^2 + E_0, \tag{7}$$

respectively.

Unlike in H_2, the quasiparticle picture breaks down in H_4. This can be seen by noting that

$$[H_4, f_k^\pm] = \left(\pm\epsilon_k H_2 - \tfrac{1}{2}\epsilon_k^2\right) f_k^\pm, \tag{8}$$

where the right-hand side is not linear in $f_k^\pm$ and involves the operator H_2. This indicates that the energy that the total system gains or loses when adding a particle with wave number k depends on the occupancy of other fermions. In this sense, a simple quasiparticle picture is not valid for H_4.

We next introduce a clean SYK model with $\mathcal{N} = 1$ supersymmetry (SUSY). The Hamiltonian is

$$H_4^{\mathrm{SUSY}} = Q^2, \quad Q = \frac{\mathrm{i}}{\sqrt{N}} \sum_{1\leqslant i_1<i_2<i_3\leqslant N} \gamma_{i_1}\gamma_{i_2}\gamma_{i_3}, \tag{9}$$

where Q is the supercharge that satisfies $Q^\dagger = Q$ and anticommutes with the fermionic parity: $\{Q, (-1)^F\} = 0$. This model is a disorder-free variant of the SUSY SYK model [44]. The model has a Majorana zero mode

$$\chi_0 = \frac{1}{\sqrt{N}} \sum_{j=1}^{N} \gamma_j, \tag{10}$$

which satisfies $(\chi_0)^2 = 1$ and $[Q, \chi_0] = 0$. To diagonalize $H_4^{\mathrm{SUSY}} = Q^2$, it is convenient to factorize Q as

$$Q = \chi_0 H_{\mathrm{free}}, \quad H_{\mathrm{free}} = \frac{\mathrm{i}}{2}\sum_{j,k} \gamma_j \tilde{\mathcal{A}}_{jk}\gamma_k, \tag{11}$$

where $\tilde{\mathcal{A}}$ is a real skew-symmetric matrix whose elements are $\tilde{\mathcal{A}}_{jk} = 1 - \frac{2|k-j|}{N}$ for $j < k$. The details of this calculation can be found in Appendix A 2. Since χ_0 and H_{free} commute, H_4^{SUSY} is written as the square of H_{free}, i.e.,

$$H_4^{\mathrm{SUSY}} = (H_{\mathrm{free}})^2. \tag{12}$$

Therefore, H_4^{SUSY} is diagonal in the basis where H_{free} is diagonal. Similar to the case of H_4, H_{free} is rewritten as

$$H_{\mathrm{free}} = \sum_{k=1}^{\frac{N}{2}-1} \varepsilon_k \left(m_k - \frac{1}{2}\right), \quad \varepsilon_k = 2\cot\frac{\vartheta_k}{2}, \tag{13}$$

where $m_k = g_k^+ g_k^-$, $\vartheta_k = 2k\pi/N$, and $g_k^\pm$ are the fermionic creation/annihilation operators defined by the Fourier

transform

$$g_k^{\pm} = \frac{1}{\sqrt{2N}} \sum_{j=1}^{N} e^{\mp \mathrm{i}(j-1)\vartheta_k} \gamma_j \tag{14}$$

for $1 \leqslant k \leqslant N/2 - 1$. They satisfy $\{g_k^s, g_{k'}^{\bar{s}'}\} = \delta_{ss'}\delta_{kk'}$. Many-body energy eigenvalues of H_4^{SUSY} specified by the occupation numbers $m_1, \ldots, m_{\frac{N}{2}-1}$ are

$$E_4^{\mathrm{SUSY}}(m_1, \ldots, m_{\frac{N}{2}-1}) = \frac{1}{4}\left(\sum_{k=1}^{\frac{N}{2}-1} (-1)^{m_k+1}\varepsilon_k\right)^2. \tag{15}$$

This expression involves only $N/2 - 1$ fermions. This is because the Majorana zero modes χ_0 and

$$\chi_{N/2} = \frac{1}{\sqrt{N}} \sum_{j=1}^{N} (-1)^{j-1}\gamma_j \tag{16}$$

do not appear in the Hamiltonian. We can define two distinct vacua $|0\rangle_+$ and $|0\rangle_-$ such that $g_k^- |0\rangle_\pm = 0$ for each k and $(-1)^F |0\rangle_\pm = \pm |0\rangle_\pm$. They are related by χ_0 since $\{\chi_0, (-1)^F\} = [H_4^{\mathrm{SUSY}}, (-1)^F] = 0$. Note that the degeneracy of these states is protected by supersymmetry. In this way, the missing degrees of freedom are restored. We can construct a tower of states by applying the creation operators g_k^+ to each vacuum.

We remark that H_4 and H_4^{SUSY} can be mapped to classical Ising models with all-to-all antiferromagnetic interactions. The spin Hamiltonian corresponding to H_4 is

$$H_4 = \sum_{k_1,k_2=1}^{N/2} J_{k_1,k_2}\sigma_{k_1}\sigma_{k_2} + E_0, \tag{17}$$

where $J_{k_1,k_2} = \frac{1}{2}\cot(\theta_{k_1}/2)\cot(\theta_{k_2}/2)$ and $\sigma_k = 2n_k - 1$. From the form of the Hamiltonian, it is obvious that each σ_k commutes with H_4. A similar representation is obtained for H_4^{SUSY}. The integrability originates from the structure that the Hamiltonian consists of the product of conserved quantities. This structure is commonly found in several other integrable models [45–47].

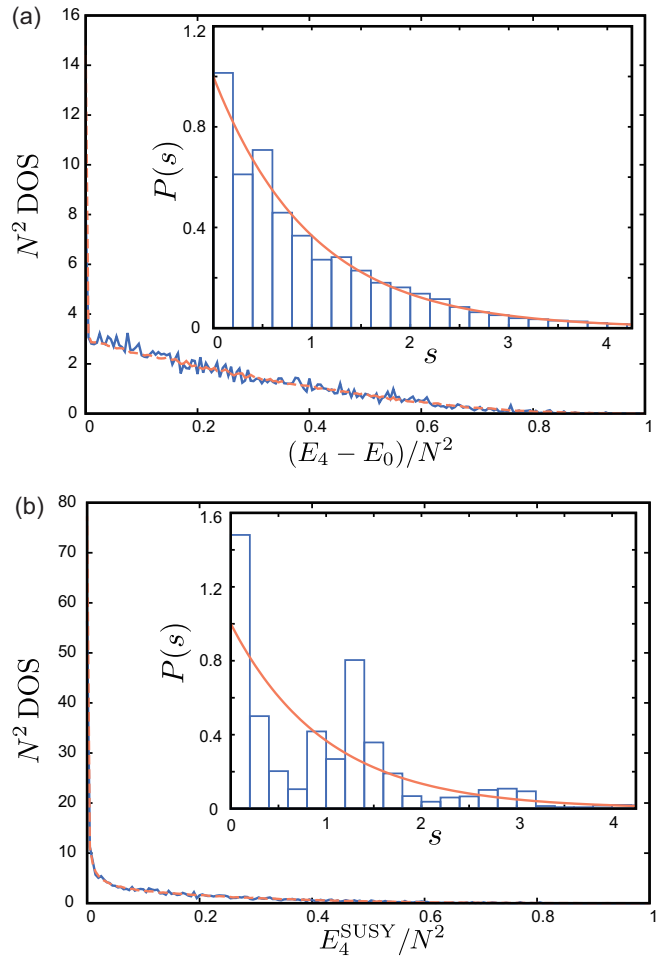

FIG. 1. Density of states for (a) H_4 and (b) H_4^{SUSY} with $N = 32$ (solid blue line) and $N = 44$ (dashed orange line). Each inset shows the corresponding level spacing statistics for $N = 44$, with s being the normalized level spacing. The energy eigenvalues in the energy windows $0.4N^2 \leqslant E_4 \leqslant 0.5N^2$ and $0.2N^2 \leqslant E_4^{\mathrm{SUSY}} \leqslant 0.3N^2$ are used for H_4 and H_4^{SUSY}, respectively. The curve $P(s) = e^{-s}$ (orange) is shown for comparison. We have reproduced the data for panel (a) for completeness, although similar results were obtained in Ref. [43].

III. LEVEL-SPACING STATISTICS

Having computed the spectra of H_4 and H_4^{SUSY}, we now study their level-spacing statistics. Let E_i $(i = 1, 2, \ldots, 2^{\frac{N}{2}})$ denote the many-body energy eigenvalues in ascending order. The many-body density of states (DOS) is defined by

$$D(E) = \frac{1}{2^{\frac{N}{2}}} \sum_{i=1}^{2^{\frac{N}{2}}} \delta(E - E_i). \tag{18}$$

Next, we examine the level-spacing statistics. In general, the mean level spacing in a system varies with energy. To enable meaningful comparisons across different energy ranges and systems, we adjust the energy spectrum locally—stretching or compressing it—so that the density of states becomes uniform within the energy range of interest [48,49]. We also remove the degeneracy since it can affect the mean level spacing. After these adjustments, we compute the level-spacing distribution $P(s)$, which is defined as the probability density for two consecutive energy levels, normalized by the mean level spacing Δ, to have a spacing s.

The numerical results of the many-body DOS and level spacing statistics for H_4 and H_4^{SUSY}, obtained using the Lorentzian representation of the delta function $\delta(x) = \delta/\pi(x^2 + \delta^2)$ with broadening $\delta = 0.1$, are shown in Fig. 1. Magnified views of the DOS are shown in Fig. 6 in Appendix A 3. For comparison, the DOS for H_2 and H_{free} are also shown in Appendix A 3.

For H_4, we find that the many-body DOS has a sharp peak at $E = E_0$ and that the level-spacing distribution follows a Poisson law [50], which is typically observed in integrable systems. This result is consistent with Ref. [43]. The many-body DOS of H_4^{SUSY} displays a divergent behavior towards $E = 0$ and also shows level concentration, which is in contrast to the sharp peak at $E = E_0$ observed for H_4. The level-spacing distribution for H_4^{SUSY} is found to be Poisson-like.

TABLE I. Number $W(\Delta E)$ of energy levels in the range $[E_0, E_0 + \Delta E]$ for H_4.

	$W(10^{-4})$	$W(10^{-3})$	$W(10^{-2})$	$W(0.02)$	$W(0.05)$	$W(0.1)$
$N = 36$	22	58	186	262	420	592
$N = 40$	74	236	730	1038	1640	2342
$N = 44$	282	922	2822	4032	6474	9032

We now analyze the many-body DOS for H_4 near the ground state in more detail. Let $W(\Delta E)$ be the number of energy levels within the range $[E_0, E_0 + \Delta E]$. The results of $W(\Delta E)$ for different values of N and ΔE are summarized in Table I. We find that these values can be approximated by

$$W(\Delta E) \simeq a \times 2^{\frac{N}{2}} \sqrt{\Delta E}, \tag{19}$$

with $a \simeq 0.007$. This result indicates that the approximate ground-state degeneracy grows exponentially with N. In the next section, we argue that the presence of a large number of states near the ground state is responsible for the residual entropy in the zero-temperature limit.

IV. THERMODYNAMIC PROPERTIES

In this section, we discuss the thermodynamic properties of the models. We denote the inverse temperature by $\beta = 1/T$. We first compute the partition function of H_4, which is defined by $Z(\beta) = \mathrm{Tr} e^{-\beta H_4}$. A more explicit expression of $Z(\beta)$ that is convenient for numerical evaluation at large N can be obtained by the Hubbard-Stratonovich (HS) transformation as

$$Z(\beta) = z(\beta) e^{-\beta E_0} \sqrt{\frac{2}{\pi\beta}} 2^{\frac{N}{2}}, \tag{20}$$

where

$$z(\beta) = \int_{-\infty}^{\infty} e^{-\frac{2x^2}{\beta}} p_N(x) dx, \quad p_N(x) = \prod_{k=1}^{N/2} \cos(\epsilon_k x). \tag{21}$$

See Appendix B 3 and for the details of the derivation.

The above integral can be evaluated numerically. Figure 2 shows $-F(\beta)/(NT) = \log Z(\beta)/N$, where $F(\beta)$ is the free energy.

At each temperature, the free energy approaches $\frac{N}{2} T \log 2$ as N increases, which suggests that the system has nonzero residual entropy. This is also understood from the fact that $z(\beta)$ in Eq. (20) is of the order of $O(\frac{1}{N})$ since $p_N(x)$ in $z(\beta)$ [Eq. (21)] is approximated as

$$p_N(x) \sim \exp\left(\frac{N}{2} \int_0^{\infty} \frac{\log|\cos x\epsilon|}{1 + (\epsilon/2)^2} \frac{d\epsilon}{\pi} \right) \sim e^{-N|x|} \tag{22}$$

in the large N limit. These results lead to a residual entropy of $s = \frac{1}{2} \log 2$, reflecting the presence of a large number of energy levels near the ground state, as discussed in the previous section. The finite residual entropy is also found in the original SYK model, which is slightly lower ($s_{\mathrm{SYK}} \sim 0.2324 = \frac{1}{2} \log(1.592)$ [17,39]) than in the present model. This discussion also applies to H_4^{SUSY}, leading to the same residual entropy as H_4. See Appendix C for details.

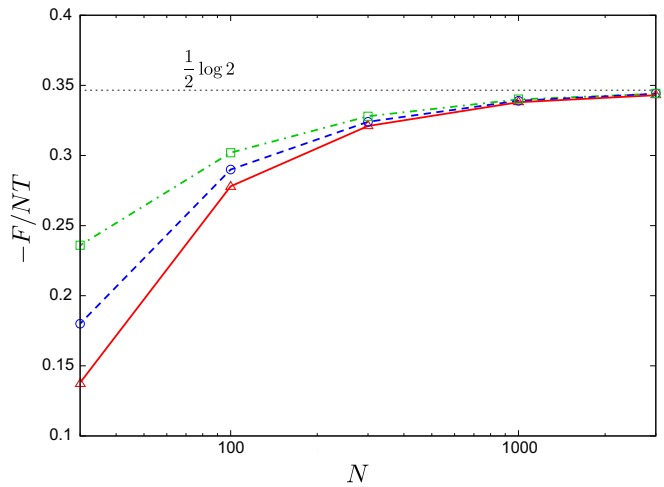

FIG. 2. Free energy of H_4 as a function of the total number of Majorana fermions N. The solid (red), dashed (blue), and dot-dashed (green) lines correspond to temperature $T = 0.1$, 1.0, and 10.0. The constant shift by E_0 is omitted.

V. TWO-POINT FUNCTIONS AND OTOCs

In this section, we study the dynamical properties of H_4. Using Eq. (8), the equation of motion of $f_k^{\pm}(t) := e^{\mathrm{i}H_4 t} f_k^{\pm} e^{-\mathrm{i}H_4 t}$ can be integrated analytically [51]. As a result, we obtain an explicit expression for the time evolution of γ_j:

$$\begin{aligned} \gamma_j(t) &:= e^{\mathrm{i}H_4 t} \gamma_j e^{-\mathrm{i}H_4 t} \\ &= \sqrt{\frac{2}{N}} \sum_{s=\pm} \sum_{k=1}^{N/2} e^{\mathrm{i}s(j-1)\theta_k} e^{-\frac{\mathrm{i}}{2}\epsilon_k^2 t} e^{\mathrm{i}s\epsilon_k H_2 t} f_k^s. \end{aligned} \tag{23}$$

Similar relations can be derived for H_4^{SUSY}, which are shown in Appendix D. We first consider the two-point function

$$G_{lm}(t) = \mathrm{Tr}[\rho\, \gamma_l(t) \gamma_m(0)], \tag{24}$$

where $\rho = \exp(-\beta H_4)/\mathrm{Tr}\exp(-\beta H_4)$ is the density matrix in thermal equilibrium at inverse temperature β. Substituting Eq. (23) to Eq. (24), we obtain

$$G_{lm}(t) = \frac{2}{N} \mathrm{Tr}\left[\rho \sum_{k=1}^{N/2} e^{-\frac{\mathrm{i}}{2}\epsilon_k^2 t} e^{\mathrm{i}(\theta_k(l-m) + \epsilon_k H_2 t)\sigma_k} \right]. \tag{25}$$

The two-point function for H_4^{SUSY}, $G_{lm}^{\mathrm{SUSY}}(t)$, is defined similarly. Figures 3(a) and 3(b) show the numerical results for the autocorrelation functions $G_{ll}(t)$ and $G_{ll}^{\mathrm{SUSY}}(t)$, corresponding to the case $l = m$. The precise definition of $G_{lm}^{\mathrm{SUSY}}(t)$ and the numerical method we use is presented in Appendix D 1.

Numerical observation suggests that $G_{ll}(t)$ and $G_{ll}^{\mathrm{SUSY}}(t)$ decay exponentially as $e^{-t/t_{\mathrm{d}}}$, up to a constant, as seen in the original SYK model [29], and then saturate after a long time. For H_4^{SUSY}, we find that $G_{ll}^{\mathrm{SUSY}}(t)$ does not completely decay and has a residual value $2/N$ due to the Majorana zero modes χ_0 [Eq. (10)] and $\chi_{N/2}$ [Eq. (16)] which do not evolve in time. See Appendix D 1 for details. This saturation time tends to become longer as N increases. The auto-correlation times are obtained as $t_{\mathrm{d}} \simeq \sqrt{\beta}/0.1$ for H_4 and $t_{\mathrm{d}} \simeq \sqrt{\beta}/0.3$ for H_4^{SUSY},

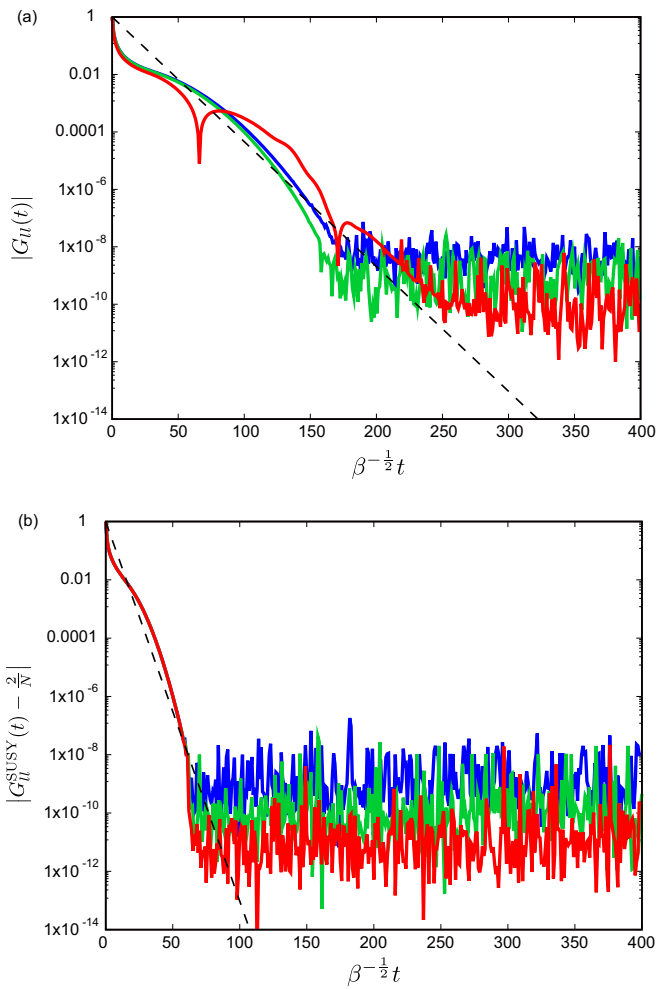

FIG. 3. Autocorrelation functions (a) $G_{ll}(t)$ and (b) $G_{ll}^{\rm SUSY}(t)$ at $N = 100$. The red, green, and blue lines represent the cases with $\beta = 0.01$, 0.1, and 1. The dashed lines in panels (a) and (b) represent the scaling $e^{-0.1t/\sqrt{\beta}}$ and $e^{-0.3t/\sqrt{\beta}}$, respectively.

which are different from $t_{\rm d} \sim \beta$ found in the original SYK model [29].

We now turn to consider the OTOC [17,29,30,40]

$$F(t,\beta) = \frac{1}{N^2}\sum_{l,m=1}^{N} {\rm Tr}\big[\rho^{\frac{1}{4}}\gamma_l(t)\rho^{\frac{1}{4}}\gamma_m(0)\rho^{\frac{1}{4}}\gamma_l(t)\rho^{\frac{1}{4}}\gamma_m(0)\big]. \tag{26}$$

Similar to the case of two-point functions, we substitute Eq. (23) to Eq. (26) and carry out the summation over l and m. After some algebra [See Appendix D 2 for details], we obtain

$$F(t,\beta) = -\frac{4}{N^2}\sum_{k_1\neq k_2} e^{-\frac{\beta}{4}(\epsilon_{k_1}^2+\epsilon_{k_2}^2)} \times {\rm Tr}\big[\rho e^{\frac{\beta}{2}(\sigma_{k_1}\epsilon_{k_1}+\sigma_{k_2}\epsilon_{k_2})H_2} e^{({\rm i}t-\frac{\beta}{4})\sigma_{k_1}\sigma_{k_2}\epsilon_{k_1}\epsilon_{k_2}}\big]. \tag{27}$$

We can calculate the OTOC for $H_4^{\rm SUSY}$ similarly, and find that its large N limit takes the form of Eq. (27) up to a constant of the order of $O(\frac{1}{N})$, with the substitutions $t \to 2t$ and $\beta \to 2\beta$ [see Appendix D 2 for details]. Below we only show the results of OTOC for H_4.

First, we consider the infinite temperature limit ($\beta = 0$), where the density matrix is proportional to the identity matrix. To compute $F(t,\beta)$ in Eq. (27), we use $\frac{2}{N}\sum_{k=1}^{N/2}(\cdots) = \int_0^\infty d\epsilon\rho(\epsilon)(\cdots)$ with $\rho(\epsilon) = \frac{1}{\pi}[1+(\frac{\epsilon}{2})^2]^{-1}$. As a result, we obtain

$$F(t,0) = -\frac{2}{\pi}f(4t) + O\left(\frac{1}{N}\right), \sim \begin{cases} -1+\frac{8}{\pi}(1-\gamma-\log 4t)t + O(t^2) & (t \ll 1), \\ -\frac{1}{2\pi t} + O\big(t^{-2}, \frac{1}{N}\big) & (t \gg 1), \end{cases} \tag{28}$$

where $f(x) = \int_0^\infty \sin(u)/(u+x)du$ is one of the auxiliary function for the trigonometric integrals and $\gamma = 0.5772\ldots$ is the Euler-Mascheroni constant. We find that the time derivative of the OTOC at $t = 0$ diverges and that the OTOC grows rapidly at early times. This rapid growth is reminiscent of those in (weakly) chaotic systems [52,53]. Note that the MSS bound $\lambda \leqslant 2\pi T$ at infinite temperature does not prohibit the divergent growth of OTOC. At late times, however, the OTOC shows t^{-1} power law decay. Such a power-law decay of OTOC is commonly seen in some integrable models [54,55] and the bipartite kicked rotor model [53].

Next, we consider the OTOC at finite temperature. By the HS transformation, we can calculate the trace in Eq. (27) and obtain

$$F(t,\beta) = -\frac{4}{zN^2}\sum_{k_1\neq k_2} e^{-\frac{\beta}{8}(\epsilon_{k_1}^2+\epsilon_{k_2}^2)}\cos\left(\epsilon_{k_1}\epsilon_{k_2}t\right) \times \int_{-\infty}^{\infty} dx e^{-\frac{2x^2}{\beta}} \prod_{k'\in K\setminus\{k_1,k_2\}} \cos x\epsilon_{k'}. \tag{29}$$

The insets of Fig. 4 show the OTOCs for H_4, $F(t,\beta)$, and for $H_4^{\rm SUSY}$, $F^{\rm SUSY}(t,\beta)$, as functions of time for different values of $T = 1/\beta$, evaluated by numerical integration. We find that the OTOCs exhibit exponential-like growth at early times. Assuming that this behavior is well described by the function $F_{\rm fit}(t) = Ae^{\lambda t} + B$, we fit the parameters A, λ, and B to the results. The fitting is carried out in the interval $[0.1\beta, 0.2\beta]$ for each temperature and the exponential parts $[F(t,\beta) - B = Ae^{\lambda t}]$ are shown in Fig. 4. Although a polynomial fit is possible, we find that the exponential fit yields more reasonable fitting parameters. See Appendix D 2 for the details of the fitting. The exponents of the observed exponential-like growth are comparable to the MSS bound $2\pi T$, which may be a precursor of quantum chaos. This exponential behavior of the OTOC is remarkable for disorder-free integrable systems without kicking/driving, although saturation of OTOCs toward zero is widely seen, e.g., see Ref. [31].

We observe that the duration of the exponential growth of the present model is about $\beta/5$ and almost independent of N, which is quite different from $\beta\log N$, the typical scrambling time of chaotic systems [56]. This may imply that a simple operator in the present model only grows to a small size in the operator space. As expected, this exponential-like behavior of the OTOC is absent in H_2 or $H_{\rm free}$, where the OTOC is -1 for any time t and does not show any scrambling behavior in the large N limit [see Appendix D 2].

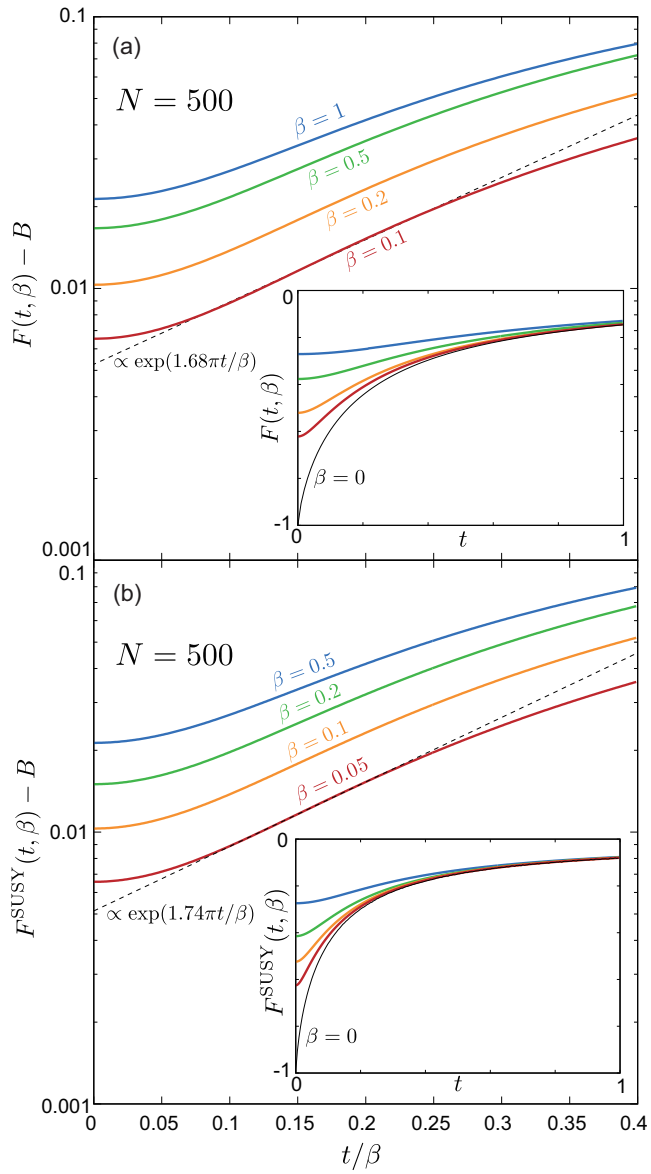

FIG. 4. OTOCs for (a) H_4 and (b) $H_4^{\rm SUSY}$ for various temperatures as functions of the rescaled time t/β, each with a constant B subtracted. The constant B is obtained by fitting the function $F_{\rm fit}(t) = Ae^{\lambda t} + B$ to numerical data over $[0.1\beta, 0.2\beta]$. Note that A and B depend on β. Insets: OTOCs without subtraction.

VI. SPECTRAL FORM FACTOR

Finally, in this section, we examine the SFF. For H_4, the SFF is defined by

$$g(t,\beta) = \left| \frac{{\rm Tr} e^{({\rm i}t-\beta)H_4}}{{\rm Tr} e^{-\beta H_4}} \right|^2, \tag{30}$$

where we do not perform disorder averages since the models we consider are free of disorder. For simplicity, we consider the case of $\beta = 0$. The early-time behavior of $g(t,0)$ can be computed analytically, as discussed in Appendix B 1. We are, however, more interested in the late-time asymptotic behavior.

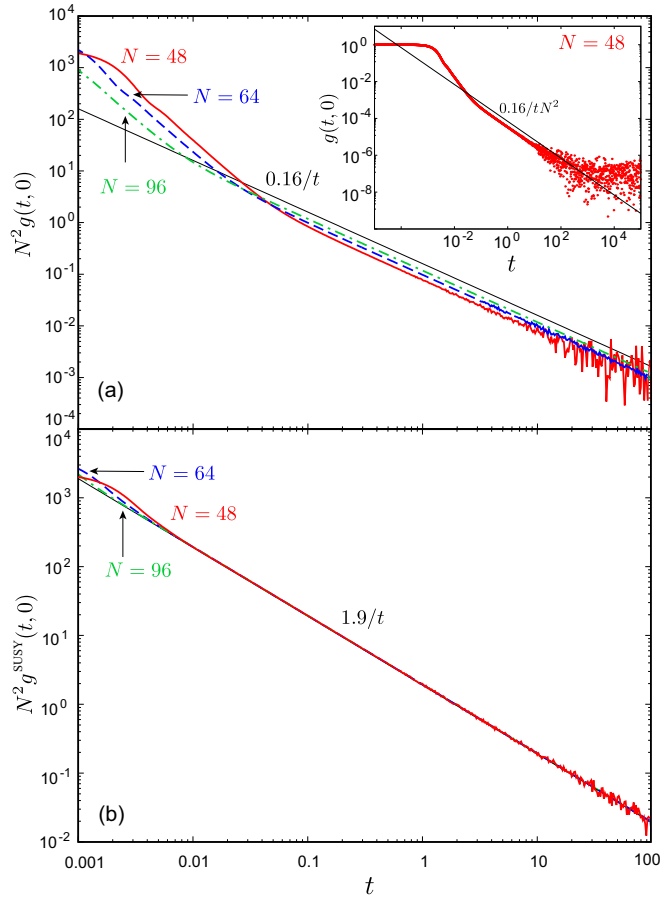

FIG. 5. SFF for (a) H_4 and (b) $H_4^{\rm SUSY}$ as functions of t. The solid (red), dashed (blue), and dot-dashed (green) lines represent the results for $N = 48$, 64, and 96, respectively. They approach $0.16/t$ with increasing N. Inset: The SFF for H_4 over a longer period of time for $N = 48$.

Using the HS transformation, we obtain

$$g(t,0) = \frac{2}{t\pi} \left| \int_{-\infty}^{\infty} e^{-{\rm i}\frac{2x^2}{t}} p_N(x) dx \right|^2. \tag{31}$$

For large N, as Eq. (22) suggests, $p_N(x)$ defined in Eq. (21) has nonnegligible values for $|x| \lesssim 1/N$. This fact is verified in Fig. 7 in Appendix B 2. In this region, the oscillating factor can be regarded as unity for $N^2 t \gg 1$. A similar expression is obtained for $H_4^{\rm SUSY}$. Furthermore, we find numerical evidence that the scaling $p_{kN}(x) \simeq p_N(kx)$ holds for a positive integer k and large N. From this relation, we can extract the scaling of SFF, $g(t,0) \sim C/N^2 t$, where the constant C is determined by numerical integration: 0.16 for H_4 and 1.9 for $H_4^{\rm SUSY}$. (See Appendix B 2 for details.)

Figures 5(a) and 5(b) show the SFF for H_4 and $H_4^{\rm SUSY}$, respectively, numerically obtained from Eq. (31) for H_4 and from its counterpart for $H_4^{\rm SUSY}$ [Eq. (B28)] for finite N. The inset shows the SFF for H_4 over a longer period of time for $N = 48$. We find that the SFF is self-averaged and that the numerical results approach the obtained scaling law at large t as N increases. Shortly before the inverse mean level spacing $\tau \sim 2^{N/2}/N^2$ (approximately 7×10^3 at $N = 48$), the

SFF begin oscillating. These results do not have a random matrix interpretation.

VII. SUMMARY

We have introduced two variants of clean SYK models and demonstrated their integrability. By exploiting this integrability, we have investigated the static and dynamical properties of the models. Notably, these models exhibit exponential behaviors in OTOCs at early times, akin to those observed in certain quantum chaotic systems, although the duration is much shorter than that for typical chaotic systems. This behavior can be interpreted as a precursor of chaos. Unlike typical chaotic systems that involve disorder or external kick terms, our models do not incorporate such elements. As anticipated, however, our analysis revealed no evidence of random matrix behavior in the level spacing statistics or SFF, indicating the integrable nature of these models. Consequently, our findings illustrate that clean SYK models provide notable examples of disorder-free quantum many-body systems displaying chaoslike behavior of OTOCs.

ACKNOWLEDGMENTS

We are grateful for fruitful discussions with Neil Dowling, Eiki Iyoda, Atsushi Iwaki, Hiroki Nakai, Pratik Nandy, Ryotaro Suzuki, and Masaki Tezuka. H.K. was supported by JSPS KAKENHI Grants No. JP18K03445, No. JP23K25790, and No. JP23K25783, MEXT KAKENHI Grant-in-Aid for Transformative Research Areas A "Extreme Universe" (KAKENHI Grant No. JP21H05191). S.O. was supported by JSPS KAKENHI Grant No. JP22KJ0988.

APPENDIX A: MANY-BODY EIGENENERGIES AND EIGENSTATES OF THE CLEAN SYK MODELS

In this Appendix, we show the detailed derivation of the energy eigenvalues and eigenstates of the clean SYK Hamiltonian H_4 in Eq. (1) and the clean SUSY SYK Hamiltonian $H_{\rm SUSY}$ in Eq. (9).

1. Clean SYK model

Here we prove Eq. (3). Consider the square of H_2:

$$(H_2)^2 = \mathrm{i}^2 \sum_{i<j} \sum_{k<l} \gamma_i \gamma_j \gamma_k \gamma_l. \tag{A1}$$

The double sum can be simplified by considering the ordering of the indices i, j, k, and l. Each term is summarized in Table II. Most of the terms in the table cancel each other, and we are left with #1, #7, and #13. As a result, we obtain the desired Eq. (3).

TABLE II. Product of Majorana operators with different order of the indices i, j, k, and l.

#	Ordering of the indices	$\gamma_i\gamma_j\gamma_k\gamma_l$
1	$i<j<k<l$	$\gamma_i\gamma_j\gamma_k\gamma_l$
2	$i<j=k<l$	$\gamma_i\gamma_l$
3	$i<k<j<l$	$-\gamma_i\gamma_k\gamma_j\gamma_l$
4	$i<k<j=l$	$-\gamma_i\gamma_k$
5	$i<k<l<j$	$\gamma_i\gamma_k\gamma_l\gamma_j$
6	$i=k<j<l$	$-\gamma_j\gamma_l$
7	$i=k<j=l$	-1
8	$i=k<l<j$	$\gamma_l\gamma_j$
9	$k<i<j<l$	$\gamma_k\gamma_i\gamma_j\gamma_l$
10	$k<i<j=l$	$\gamma_k\gamma_i$
11	$k<i<l<j$	$-\gamma_k\gamma_i\gamma_l\gamma_j$
12	$k<i=l<j$	$-\gamma_k\gamma_j$
13	$k<l<i<j$	$\gamma_k\gamma_l\gamma_i\gamma_j$

It is clear from Eq. (3) that the basis that diagonalizes H_2 also diagonalizes H_4. The quadratic Hamiltonian H_2 is diagonalized as follows [43]. We rewrite H_2 in a matrix form

$$H_2 = \frac{\mathrm{i}}{2} \sum_{jk} \mathcal{A}_{jk} \gamma_j \gamma_k, \tag{A2}$$

where $\mathcal{A}$ is an $N\times N$ real skew symmetric matrix, whose components are

$$\mathcal{A}_{jk} = \begin{cases} 1 & (j<k) \\ 0 & (j=k) \\ -1 & (j>k) \end{cases}. \tag{A3}$$

Since the matrix $\mathcal{A}$ is a circulant matrix with antiperiodic boundary conditions, $\mathcal{A}$ is diagonalized by

$$\boldsymbol{u}_k = \frac{1}{\sqrt{N}} \left(1, \quad e^{\mathrm{i}\theta_k}, \quad e^{\mathrm{i}2\theta_k}, \quad \ldots, \quad e^{\mathrm{i}(N-1)\theta_k}\right)^{\mathrm{T}}, \tag{A4}$$

with $k = 1, 2, \cdots, N$ and $\theta_k = (2k-1)\pi/N$. The eigenvalue of $\mathcal{A}$ corresponding to $\boldsymbol{u}_k$ is obtained as $\mathrm{i}\cot\frac{\theta_k}{2}$. Using $\boldsymbol{u}_k$, we can construct an orthogonal matrix $\mathcal{O}$ such that

$$\mathcal{O}^{\mathrm{T}} \mathcal{A} \mathcal{O} = \bigoplus_{k=1}^{\frac{N}{2}} \begin{pmatrix} 0 & \cot\frac{\theta_k}{2} \\ -\cot\frac{\theta_k}{2} & 0 \end{pmatrix}. \tag{A5}$$

Explicitly, it is given by

$$\begin{aligned} \mathcal{O} &= \left(\frac{\boldsymbol{u}_1 + \boldsymbol{u}_N}{\sqrt{2}}, \frac{\boldsymbol{u}_1 - \boldsymbol{u}_N}{\sqrt{2}\mathrm{i}}, \frac{\boldsymbol{u}_2 + \boldsymbol{u}_{N-1}}{\sqrt{2}}, \frac{\boldsymbol{u}_2 - \boldsymbol{u}_{N-1}}{\sqrt{2}\mathrm{i}}, \ldots, \frac{\boldsymbol{u}_{\frac{N}{2}} + \boldsymbol{u}_{\frac{N}{2}+1}}{\sqrt{2}}, \frac{\boldsymbol{u}_{\frac{N}{2}} - \boldsymbol{u}_{\frac{N}{2}+1}}{\sqrt{2}\mathrm{i}} \right) \\ &= \sqrt{\frac{2}{N}} \begin{pmatrix} 1 & 0 & \cdots & 1 & 0 \\ \cos\theta_1 & \sin\theta_1 & \cdots & \cos\theta_{\frac{N}{2}} & \sin\theta_{\frac{N}{2}} \\ \vdots & \vdots & & \vdots & \vdots \\ \cos(N-1)\theta_1 & \sin(N-1)\theta_1 & \cdots & \cos(N-1)\theta_{\frac{N}{2}} & \sin(N-1)\theta_{\frac{N}{2}} \end{pmatrix}, \end{aligned} \tag{A6}$$

where we have used the relation $\boldsymbol{u}_{N-k+1} = \boldsymbol{u}_k^*$.

This transformation defines a new set of Majorana fermions

$$\psi_{2k-1} = \sqrt{\frac{2}{N}} \sum_{j=1}^{N} \cos[(j-1)\theta_k]\gamma_j, \tag{A7}$$

$$\psi_{2k} = \sqrt{\frac{2}{N}} \sum_{j=1}^{N} \sin[(j-1)\theta_k]\gamma_j, \tag{A8}$$

in terms of which the quadratic Hamiltonian H_2 is expressed as

$$H_2 = \frac{\mathrm{i}}{2} \sum_{k=1}^{\frac{N}{2}} \cot\frac{\theta_k}{2} (\psi_{2k-1}\psi_{2k} - \psi_{2k}\psi_{2k-1}). \tag{A9}$$

To rewrite H_2 in a diagonal form, we introduce

$$f_k^{\pm} = \frac{\psi_{2k-1} \mp \mathrm{i}\psi_{2k}}{2} \tag{A10}$$

with anticommutation relations $\{f_k^{s_1}, f_{k'}^{\bar{s}_2}\} = \delta_{s_1,s_2}\delta_{k,k'}$, where $\bar{s}$ $(s = +, -)$ is a short-hand notation for $-s$. In terms of complex fermions, H_2 takes the form Eq. (5), which leads to the energy eigenvalues $E_2(n_1, \ldots, n_{\frac{N}{2}})$ [Eq. (6)] and $E_4(n_1, \ldots, n_{\frac{N}{2}})$ [Eq. (7)], where $n_k = 0$ or 1 is the occupation number for the fermion corresponding to ϵ_k. In this fermionic representation, the maximum number of k's is $k_{\max} = \frac{N}{2}$.

2. Clean SUSY SYK model

The Hamiltonian and the supercharge defined in Eq. (9) satisfy the $\mathcal{N} = 1$ supersymmetry algebra

$$Q^{\dagger} = Q, \quad \{Q, (-1)^F\} = 0. \tag{A11}$$

Here $(-1)^F = \mathrm{i}^{N/2}\gamma_1\gamma_2\cdots\gamma_N$ is the fermionic parity. We find a Majorana zero mode χ_0 [Eq. (10)] that commute with the Hamiltonian H_4^{SUSY}, which follows from $[Q, \chi_0] = 0$. Using χ_0, we factorize Q as shown below:

$$\begin{aligned} Q &= (\chi_0)^2 Q \\ &= \chi_0 \frac{\mathrm{i}}{N} \sum_{l=1}^{N} \sum_{1\leqslant i<j<k\leqslant N} \gamma_l\gamma_i\gamma_j\gamma_k \\ &= \chi_0 \frac{\mathrm{i}}{N} \Bigg(\sum_{1\leqslant l<i<j<k\leqslant N} + \sum_{1\leqslant i<l<j<k\leqslant N} + \sum_{1\leqslant i<j<l<k\leqslant N} \\ &\quad + \sum_{1\leqslant i<j<k<l\leqslant N} \Bigg) \gamma_l\gamma_i\gamma_j\gamma_k \\ &\quad + \chi_0 \frac{\mathrm{i}}{N} \sum_{1\leqslant i<j<k\leqslant N} [\gamma_i\gamma_i\gamma_j\gamma_k + \gamma_j\gamma_i\gamma_j\gamma_k + \gamma_k\gamma_i\gamma_j\gamma_k]. \end{aligned} \tag{A12}$$

Since the Majorana fermions anticommute on different sites, the first term vanishes. The last term simplifies to $\chi_0 H_{\mathrm{free}}$, or equivalently, $H_{\mathrm{free}}\chi_0$ with

$$H_{\mathrm{free}} = \frac{\mathrm{i}}{2} \sum_{j,k} \tilde{\mathcal{A}}_{jk}\gamma_j\gamma_k, \quad \tilde{\mathcal{A}}_{jk} = \begin{cases} 1 - \frac{2|k-j|}{N} & (j < k) \\ 0 & (j = k) \\ -1 + \frac{2|k-j|}{N} & (j > k) \end{cases}. \tag{A13}$$

Note that the commutation relation $[\chi_0, H_{\mathrm{free}}] = 0$ follows from $[Q, \chi_0] = 0$. To sum up, we have $Q = \chi_0 H_{\mathrm{free}}$ and obtain a simple relation Eq. (12) between H_4^{SUSY} and H_{free}, which is analogous to Eq. (3). The Hamiltonian H_4^{SUSY} consists of the square of three-body interaction; however, Eq. (12) indicates that H_4^{SUSY} contains four-body terms at most. Furthermore, the quadratic terms vanish in H_4^{SUSY} due to the antisymmetric property of the matrix $\tilde{\mathcal{A}}$ in Eq. (A13). Therefore, H_4^{SUSY} consists only of the quartic terms up to a constant.

We now diagonalize H_{free}. Since $\tilde{\mathcal{A}}$ is a circulant matrix with periodic boundary conditions, $\tilde{\mathcal{A}}$ is diagonalized by the following eigenvectors:

$$\boldsymbol{v}_k = \frac{1}{\sqrt{N}} \left(1, \quad e^{\mathrm{i}\vartheta_k}, \quad e^{\mathrm{i}2\vartheta_k}, \quad \ldots, \quad e^{\mathrm{i}(N-1)\vartheta_k}\right)^{\mathrm{T}}, \tag{A14}$$

for $k = 0, 1, \ldots, N-1$ with $\vartheta_k = 2k\pi/N$, and the corresponding eigenvalues are obtained as

$$\lambda_k = \begin{cases} 0 & \left(k = 0 \text{ or } k = \frac{N}{2}\right) \\ \mathrm{i}\cot\frac{\vartheta_k}{2} & (\text{otherwise}) \end{cases}. \tag{A15}$$

This result implies another Majorana zero mode $\chi_{N/2}$ [Eq. (16)], corresponding to $\boldsymbol{v}_{N/2}$ as well as χ_0, corresponding to $\boldsymbol{v}_0$. Similar to the case of the clean SYK model, the orthogonal matrix $\tilde{\mathcal{O}}$ defined by

$$\begin{aligned} \tilde{\mathcal{O}} = \Bigg(&\frac{\boldsymbol{v}_1 + \boldsymbol{v}_{N-1}}{\sqrt{2}}, \frac{\boldsymbol{v}_1 - \boldsymbol{v}_{N-1}}{\sqrt{2}\mathrm{i}}, \frac{\boldsymbol{v}_2 + \boldsymbol{v}_{N-2}}{\sqrt{2}}, \frac{\boldsymbol{v}_2 - \boldsymbol{v}_{N-2}}{\sqrt{2}\mathrm{i}}, \\ &\ldots, \frac{\boldsymbol{v}_{\frac{N}{2}-1} + \boldsymbol{v}_{\frac{N}{2}+1}}{\sqrt{2}}, \frac{\boldsymbol{v}_{\frac{N}{2}-1} - \boldsymbol{v}_{\frac{N}{2}+1}}{\sqrt{2}\mathrm{i}}, \boldsymbol{v}_0, \boldsymbol{v}_{\frac{N}{2}} \Bigg) \end{aligned} \tag{A16}$$

reduces $\tilde{\mathcal{A}}$ to a canonical form:

$$\tilde{\mathcal{O}}^{\mathrm{T}}\tilde{\mathcal{A}}\tilde{\mathcal{O}} = \left(\bigoplus_{k=1}^{\frac{N}{2}-1} \begin{pmatrix} 0 & \cot\frac{\vartheta_k}{2} \\ -\cot\frac{\vartheta_k}{2} & 0 \end{pmatrix} \right) \oplus \begin{pmatrix} 0 & 0 \\ 0 & 0 \end{pmatrix}. \tag{A17}$$

Consequently, we can rewrite the Hamiltonian as

$$H_{\mathrm{free}}^{\mathrm{SUSY}} = \sum_{k=1}^{\frac{N}{2}-1} \varepsilon_k \left(g_k^+ g_k^- - \frac{1}{2} \right), \quad \varepsilon_k = 2\cot\frac{\vartheta_k}{2}, \tag{A18}$$

where

$$g_k^{\pm} = \frac{\chi_{2k-1} \mp \mathrm{i}\chi_{2k}}{2} \quad \text{for } k = 1, \ldots \frac{N}{2} - 1, \tag{A19}$$

with

$$\chi_{2k-1} = \sqrt{\frac{2}{N}} \sum_{j=1}^{N} \cos[(j-1)\vartheta_k]\gamma_j, \tag{A20}$$

$$\chi_{2k} = \sqrt{\frac{2}{N}} \sum_{j=1}^{N} \sin[(j-1)\vartheta_k]\gamma_j, \tag{A21}$$

obeying the anticommutation relations $\{g_k^{s_1}, g_{k'}^{\bar{s}_2}\} = \delta_{s_1,s_2}\delta_{k,k'}$. It then follows from Eq. (12) that the many-body energy eigenvalue of H_4^{SUSY} is given by $E_4^{\mathrm{SUSY}}(m_1, \ldots, m_{\frac{N}{2}-1})$ [Eq. (15)], where $m_k = 0$ or 1 is the occupation number for the fermion corresponding to ε_k. In this fermionic representation, the maximum number of k's is $k_{\max} = \frac{N}{2} - 1$.

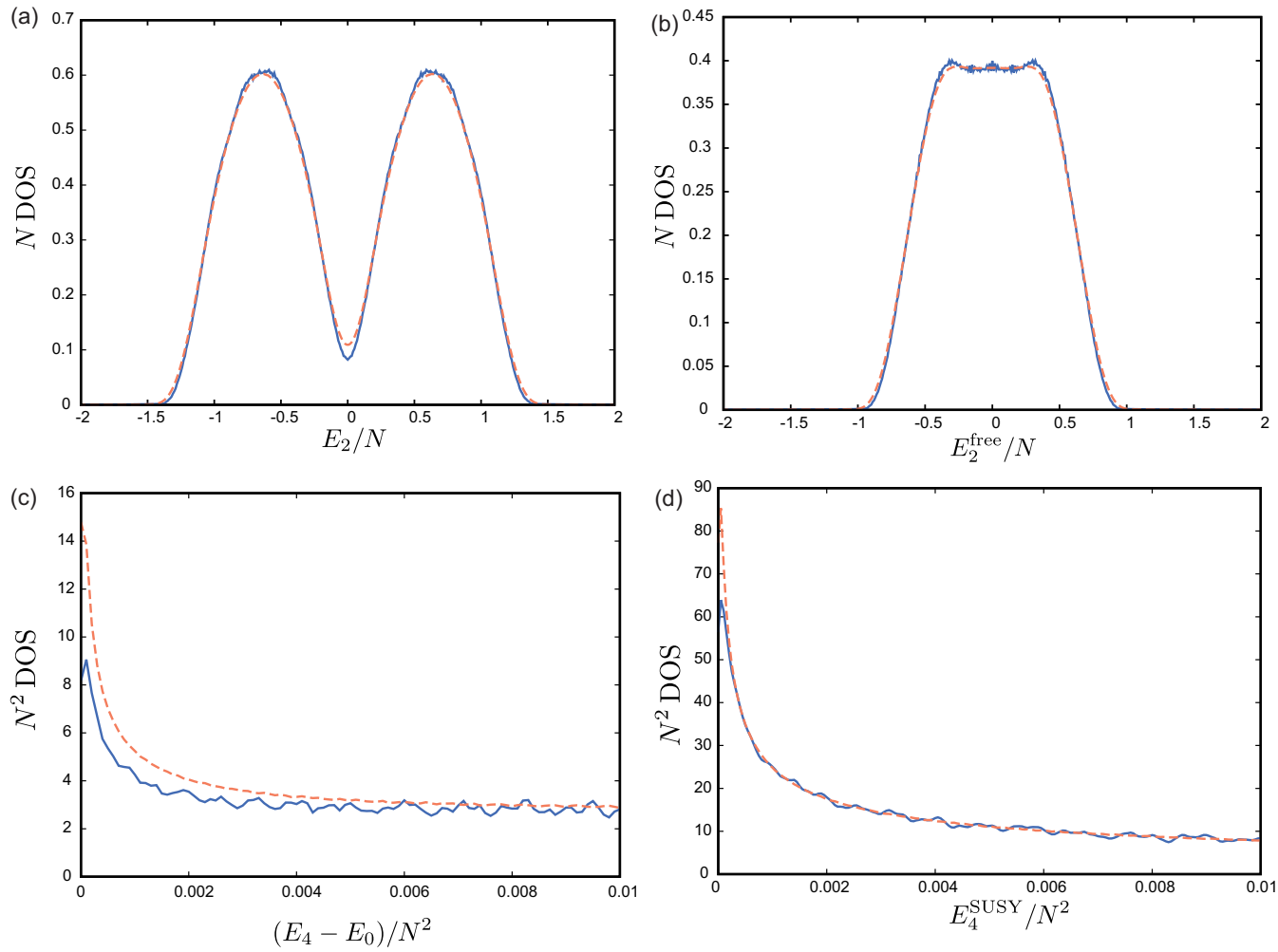

FIG. 6. Density of states for (a) H_2, (b) $H_{\rm free}$, (c) H_4, and (d) $H_4{}^{\rm SUSY}$ with $N = 32$ (solid blue line) and $N = 44$ (dashed orange line). E_2, $E_2^{\rm free}$, E_4, and $E_4^{\rm SUSY}$ represent the energy eigenvalues for H_2, $H_{\rm free}$, H_4, and $H_4^{\rm SUSY}$, respectively. Note that the normalizations are different. Panels (c) and (d) present the magnified views of Figs. 1(a) and 1(b), respectively.

3. Many-body DOS and level statistics

The many-body DOS for H_2, $H_{\rm free}$, H_4, and $H_4^{\rm SUSY}$ are shown in Figs. 6(a), 6(b), 6(c), and 6(d), respectively, with magnified views provided for the latter two. The many-body DOS for H_2 exhibits a double-peak structure, whereas that for $H_{\rm free}$ shows a flat peak. The squared Hamiltonians H_4 and $H_4^{\rm SUSY}$ demonstrate a significant level concentration near the ground state.

APPENDIX B: SPECTRAL FORM FACTORS

In this Appendix, we show the detailed calculations of the SFF of H_4 and $H_4^{\rm SUSY}$. The SFF of H_4 is defined in Eq. (30). To proceed, it is more convenient to rewrite it as

$$g(t,\beta) = \left| \frac{{\rm Tr} e^{({\rm i}t-\beta)(H_4-E_0)}}{Z_0(\beta)} \right|^2, \tag{B1}$$

where

$$Z_0(\beta) = {\rm Tr} e^{-\beta(H_4-E_0)} = {\rm Tr} e^{-\frac{\beta}{2}(H_2)^2}. \tag{B2}$$

The partition function of H_4, i.e., ${\rm Tr} e^{-\beta H_4}$, and $Z_0(\beta)$ are related to each other by $Z(\beta) = e^{-\beta E_0} Z_0(\beta)$. The SFF of $H_4^{\rm SUSY}$ is defined as

$$g^{\rm SUSY}(t,\beta) = \left| \frac{{\rm Tr} e^{({\rm i}t-\beta)H_4^{\rm SUSY}}}{Z^{\rm SUSY}(\beta)} \right|^2, \tag{B3}$$

where

$$Z^{\rm SUSY}(\beta) = {\rm Tr} e^{-\beta H_4^{\rm SUSY}} = {\rm Tr} e^{-\beta (H_{\rm free})^2}. \tag{B4}$$

We show the results for early-time and large N behavior at the infinite tempeature in Appendices B 1 and B 2, respectively. In these cases, we have $Z(\beta = 0) = Z^{\rm SUSY}(\beta = 0) = 2^{\frac{N}{2}}$. We also give expressions for SFFs at finite temperature in Appendix B 3.

1. Small t expansion

Here, we show that the power series expansion of $g(t, \beta = 0)$ up to t^2 is given by

$$g(t,0) = 1 - \binom{N}{4} t^2 + O(t^4), \tag{B5}$$

which indicates that $g(t,0)$ decays faster at early times with increasing N. To derive the above expression, we expand the numerator in Eq. (B1) in t as

$$\mathrm{Tr}\, e^{\mathrm{i}tH_4} = 1 + \mathrm{i}t\,\mathrm{Tr}\, H_4 + \frac{(\mathrm{i}t)^2}{2!}\mathrm{Tr}\,(H_4)^2 + \frac{(\mathrm{i}t)^3}{3!}\mathrm{Tr}(H_4)^3 + O(t^4). \tag{B6}$$

We show below that

$$\mathrm{Tr}\, H_4 = 0, \tag{B7}$$

$$\mathrm{Tr}\,(H_4)^2 = 2^{\frac{N}{2}}\binom{N}{4}, \tag{B8}$$

$$\mathrm{Tr}\,(H_4)^3 = 2^{\frac{N}{2}}\cdot 6\binom{N}{6}. \tag{B9}$$

To evaluate these traces, it is convenient to use another expression of the Hamiltonian:

$$H_4 = \frac{1}{4}\sum_{a<b}\sigma_{k_a}\sigma_{k_b}\epsilon_{k_a}\epsilon_{k_b}, \tag{B10}$$

where $\sigma_{k_a} := 2n_{k_a} - 1$. This expression leads to $\mathrm{Tr}H_4 = 0$. This also follows from the original expression Eq. (1) using the cyclicity of the trace and the anticommutation relation of Majorana fermions.

Next, we evaluate $\mathrm{Tr}(H_4)^2$. In terms of the spin variables, it can be expressed as

$$\mathrm{Tr}(H_4)^2 = \frac{1}{4^2}\sum_{\sigma_1,\cdots,\sigma_{N/2}=\pm1}\sum_{a<b}\sum_{c<d}\sigma_{k_a}\sigma_{k_b}\sigma_{k_c}\sigma_{k_d}\epsilon_{k_a}\epsilon_{k_b}\epsilon_{k_c}\epsilon_{k_d}. \tag{B11}$$

In the sum, the terms that satisfy $a = c$ and $b = d$ only remain, which leads to Eq. (B8).

In the third order, similarly, we have

$$\mathrm{Tr}(H_4)^3 = \frac{1}{4^3}\sum_{\sigma_1,\ldots,\sigma_{N/2}=\pm1}\sum_{a<b}\sum_{c<d}\sum_{e<f} \times \sigma_{k_a}\sigma_{k_b}\sigma_{k_c}\sigma_{k_d}\sigma_{k_e}\sigma_{k_f}\epsilon_{k_a}\epsilon_{k_b}\epsilon_{k_c}\epsilon_{k_d}\epsilon_{k_e}\epsilon_{k_f}. \tag{B12}$$

The terms that satisfy one of the following conditions,

$$\begin{aligned} &a = c < b = e < d = f\\ &a = c < d = e < b = f\\ &a = e < b = c < d = f\\ &a = e < c = f < b = d\\ &c = e < a = d < b = f\\ &c = e < a = f < b = d, \end{aligned} \tag{B13}$$

give nonzero contributions and other terms vanish after taking the summation over $\sigma_1,\ldots,\sigma_{N/2}$. Therefore, we obtain

$$\mathrm{Tr}(H_4)^3 = \frac{2^6}{4^3}6\cdot 2^{\frac{N}{2}}\sum_{1\leqslant a<b<c\leqslant\frac{N}{2}}\prod_{i=a,b,c}\cot^2\left(\frac{2k_i-1}{2N}\pi\right). \tag{B14}$$

This expression can be simplified using the following identity which holds for $1\leqslant j\leqslant n$:

$$\sum_{1\leqslant i_1<i_2<\cdots<i_j\leqslant n}\prod_{m=1}^{j}\cot^2\left(\frac{2k_{i_m}-1}{4n}\pi\right) = \binom{2n}{2j}. \tag{B15}$$

Proof. We begin with the identity

$$(e^{\mathrm{i}\theta_j})^{2n} = (\cos\theta_j + \mathrm{i}\sin\theta_j)^{2n}, \tag{B16}$$

with $\theta_j = \frac{2j-1}{4n}\pi$. Comparing the real parts of both sides, we obtain

$$0 = \sum_{k=0}^{n}\binom{2n}{2k}(-1)^{n-k}(\cos\theta_j)^{2k}(\sin\theta_j)^{2(n-k)}, \tag{B17}$$

which yields

$$\sum_{k=0}^{n}\binom{2n}{2k}(\cot\theta_j)^{2k}(-1)^{n-k} = 0. \tag{B18}$$

Here, we have used the fact that $\sin\theta_j \neq 0$ for $1\leqslant j\leqslant n$. We now consider an nth-order polynomial

$$f(x) = \sum_{k=0}^{n}(-1)^{n-k}\binom{2n}{2k}x^k. \tag{B19}$$

Then, we see that $(\cot\theta_j)^2$ $(j = 1,\ldots,N)$ are distinct roots of the polynomial $f(x)$. Therefore, $f(x)$ is factorized as

$$f(x) = \prod_{j=1}^{n}[x - (\cot\theta_j)^2]. \tag{B20}$$

Comparing the coefficients of x^k, we obtain Eq. (B15). ■

Substituting Eq. (B15) into Eq. (B14) yields the desired result Eq. (B9). Then substituting the obtained traces into the series expansion of $g(t,0) = |\mathrm{Tr}e^{\mathrm{i}tH_4}|^2/2^N$, we get Eq. (B5).

2. Large N behaviors

Next, we consider the large N behaviors. Using the Hubbard-Stratonovich (HS) transformation

$$e^{\mathrm{i}tA^2} = e^{\frac{\mathrm{i}\pi}{4}}\sqrt{\frac{t}{\pi}}\int_{-\infty}^{\infty}e^{-\mathrm{i}tx^2+2\mathrm{i}txA}dx, \tag{B21}$$

for Hermitian A with the assumption that time t is real, we obtain

$$\begin{aligned} 2^{-\frac{N}{2}}\mathrm{Tr}e^{\mathrm{i}H_4t} &= e^{-\mathrm{i}\frac{N(N-1)}{4}t}e^{\frac{\mathrm{i}\pi}{4}}\sqrt{\frac{t}{\pi}}\frac{1}{2^{\frac{N}{2}}}\sum_{\sigma_1,\ldots,\sigma_{N/2}=\pm1}\int_{-\infty}^{\infty}e^{-\mathrm{i}tx^2}\\ &\quad\times e^{\mathrm{i}tx\cdot\frac{1}{\sqrt{2}}\sum_k\sigma_k\varepsilon_k}dx\\ &= e^{-\mathrm{i}\frac{N(N-1)}{4}t}e^{\frac{\mathrm{i}\pi}{4}}\sqrt{\frac{2}{t\pi}}\int_{-\infty}^{\infty}e^{-\mathrm{i}\frac{2u^2}{t}}p_N(u)du, \end{aligned} \tag{B22}$$

where

$$p_N(x) = \prod_{k=1}^{\frac{N}{2}}\cos(\epsilon_k x). \tag{B23}$$

Here, we examine the property of $p_N(x)$. We consider the single-particle DOS $D_1(\epsilon)$,

$$\begin{aligned} D_1(\epsilon) &= \frac{2}{N}\sum_{k=1}^{\frac{N}{2}} \delta(\epsilon - \epsilon_k) \\ &\simeq 2\int_0^{\frac{1}{2}} dk\,\delta(\epsilon - 2\cot(k\pi)) \\ &= \frac{1}{\pi}\frac{1}{1+\epsilon^2/4}. \end{aligned} \tag{B24}$$

From this, we find that

$$\begin{aligned} |p_N(x)| &= e^{\sum_{k=1}^{k_{\max}} \log|\cos\epsilon_k x|} \\ &\simeq \exp\left(\frac{N}{2}\frac{1}{\pi}\int_0^\infty \frac{4|x|}{\epsilon^2+4x^2}\log|\cos\epsilon|d\epsilon\right) \\ &= \left(\frac{1+e^{-4|x|}}{2}\right)^{\frac{N}{2}} \\ &\to e^{-N|x|} =: \tilde{p}_N(x) \quad (N\to\infty). \end{aligned} \tag{B25}$$

The function $p_N(x)$ and its approximation $\tilde{p}_N(x)$ are shown in Fig. 7. This result indicates that $p_N(x)$ decays almost exponentially over a range $[0, 1/N]$. Furthermore, our numerical results suggest an approximate scaling:

$$p_{kN}(x) \sim p_N(kx), \tag{B26}$$

with positive integer k for large N. By the replacement of $N = kN_0$ with N_0 being the large positive integer, we can extract the scaling of $g(t,0)$ at large t and N,

$$\begin{aligned} g(t,0) &= \frac{2}{\pi t}\left|\int_{-\infty}^{\infty} e^{-\mathrm{i}\frac{2u^2}{t}} p_N(u)du\right|^2 \\ &\simeq \frac{8}{\pi t}\left(\int_0^\Lambda p_{N_0}(ku)du\right)^2 \\ &= \frac{8}{\pi t N^2}\left(N_0\int_0^{k\Lambda} p_{N_0}(u)du\right)^2 \\ &= \frac{0.16}{tN^2}, \end{aligned} \tag{B27}$$

where we have performed a numerical integration with $N_0 = 1000$ and sufficiently large cutoff Λ. The approximate functional form $p_N(x) \sim e^{-Nx}$ has been used solely to justify the truncation of the integral in the second line in Eq. (B27) and we use the correct form for the numerical integration in the third line. The result exhibits a power-law decay, which is in good agreement with the fully numerical result shown in Fig. 5(a).

For H_4^{SUSY}, similarly, we obtain

$$2^{-\frac{N}{2}}\mathrm{Tr}e^{\mathrm{i}H_4^{\mathrm{SUSY}}t} = e^{\mathrm{i}\frac{\pi}{4}}\frac{1}{\sqrt{\pi t}}\int_{-\infty}^{\infty} du\, e^{-\mathrm{i}\frac{u^2}{t}} p_N^{\mathrm{SUSY}}(u), \tag{B28}$$

where we have introduced

$$p_N^{\mathrm{SUSY}}(x) = \prod_{k=1}^{\frac{N}{2}-1}\cos(\varepsilon_k x), \tag{B29}$$

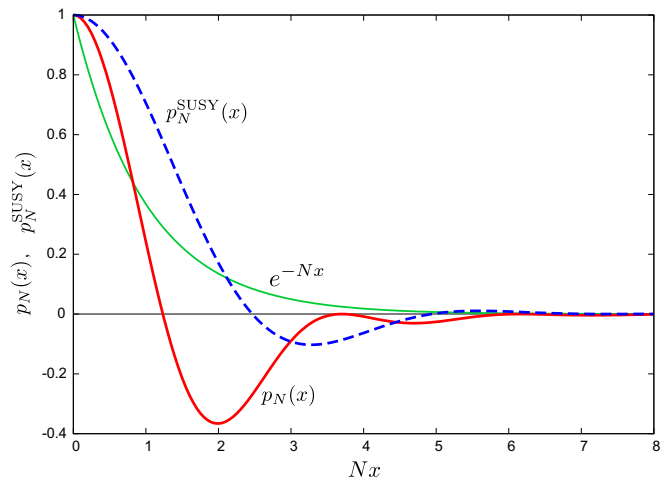

FIG. 7. Function $p_N(x)$ (red solid line), $p_N^{\mathrm{SUSY}}(x)$ (blue dashed line), and their approximation $\tilde{p}_N(x)$ (green solid line) with $N = 1000$. With this scaling of the axes, the shape of the graph does not change as long as N is sufficiently large. This fact indicates that $p_{kN}(x) \sim p_N(kx)$ and $p_{kN}^{\mathrm{SUSY}}(x) \sim p_N^{\mathrm{SUSY}}(kx)$.

which is also shown in Fig. 7. This function is also approximated as $p_N^{\mathrm{SUSY}}(x) \simeq e^{-Nx} = \tilde{p}_N(x)$, and we find an approximate scaling

$$p_{Nk}^{\mathrm{SUSY}}(x) \sim p_N^{\mathrm{SUSY}}(kx). \tag{B30}$$

Similar to the analysis of $g(t,0)$, we assume this scaling relation and obtain

$$g^{\mathrm{SUSY}}(t,0) \simeq \frac{1.9}{tN^2} \tag{B31}$$

by numerical integration. The fully numerical result for SFF of H_4^{SUSY} and its approximation Eq. (B31) are shown in Fig. 5(b).

These results clearly show that the SFFs for H_4 and H_4^{SUSY} at large t and N are proportional to $1/N^2t$. The SFFs start to deviate from $0.16/N^2t$ and $1.9/N^2t$ at sufficiently late times. The time at which the deviation occurs increases with N.

3. Spectral form factor at finite temperature

Finally, we consider $g(t,\beta)$ and $g^{\mathrm{SUSY}}(t,\beta)$ at finite temperature. We introduce the general HS transformation,

$$e^{-\alpha A^2} = \frac{e^{-\frac{\mathrm{i}}{2}\mathrm{Arg}\alpha}}{\sqrt{|\alpha|\pi}}\int_{-\infty}^{\infty} dx\, e^{-\frac{x^2}{\alpha}+2\mathrm{i}Ax}, \tag{B32}$$

for $\mathrm{Re}\,\alpha \geqslant 0$ with Hermitian A. By the HS transformation, we obtain numerically tractable expressions for $Z_0(\beta)$ and $Z^{\mathrm{SUSY}}(\beta)$ as

$$Z_0(\beta) = z(\beta)\sqrt{\frac{2}{\pi\beta}}2^{\frac{N}{2}} \tag{B33}$$

and

$$Z^{\mathrm{SUSY}}(\beta) = z^{\mathrm{SUSY}}(\beta)\frac{1}{\sqrt{\pi\beta}}2^{\frac{N}{2}}, \tag{B34}$$

with

$$z(\beta) = \int_{-\infty}^{\infty} e^{-\frac{2x^2}{\beta}} p_N(x)dx \tag{B35}$$

and

$$z^{\mathrm{SUSY}}(\beta) = \int_{-\infty}^{\infty} e^{-\frac{x^2}{\beta}} p_N^{\mathrm{SUSY}}(x)dx. \tag{B36}$$

Using Eqs. (B1), (B3), and (B33)–(B36), we obtain

$$g_N(t,\beta) = \frac{1}{z(\beta)^2}\frac{\beta}{\sqrt{t^2+\beta^2}}\left|\int_{-\infty}^{\infty} dx e^{-\frac{2x^2}{\beta-it}} p(x)\right|^2 \tag{B37}$$

for H_4 and

$$g_N^{\mathrm{SUSY}}(t,\beta)=\frac{1}{(z^{\mathrm{SUSY}}(\beta))^2}\frac{\beta}{\sqrt{t^2+\beta^2}}\left|\int_{-\infty}^{\infty} dx e^{-\frac{x^2}{\beta-it}} p^{\mathrm{SUSY}}(x)\right|^2 \tag{B38}$$

for H_4^{SUSY}.

APPENDIX C: THERMODYNAMIC PROPERTIES

In this Appendix, we detailed calculations of the thermodynamic properties of H_4 and H_4^{SUSY}. For H_4, in the following, we use the partition function $Z_0(\beta)$ [Eq. (B2)] to remove the constant shift of the total energy, E_0. In the high-temperature limit $\beta \to 0$, the Gaussian distribution approaches $e^{-\frac{2u^2}{\beta}} \to \sqrt{\beta\pi/2}\delta(u)$. Therefore, the free energy F is given by

$$F(\beta) = -\frac{1}{\beta}\log Z_0(\beta) \sim -\frac{NT}{2}\log 2 \quad (\beta \to 0), \tag{C1}$$

which is the expected behavior in the high-temperature limit.

Next, we consider the large N limit. We evaluate $z(\beta)$ using the approximation $p_N(x) \sim \tilde{p}_N(x)$ and the asymptotic expansion of the error function as

$$z(\beta) \sim 2\int_0^{\infty} e^{-\frac{2x^2}{\beta}} e^{-Nx} dx = \frac{2}{N} + O\left(\frac{1}{N^3}\right). \tag{C2}$$

Although the approximation we have used is not highly accurate as seen in Fig. 7, such a difference does not affect thermodynamic quantities. Combining Eq. (C2) with Eq. (B33) we obtain

$$F(\beta) \sim -\frac{NT}{2}\log 2 \quad (N \to \infty), \tag{C3}$$

which indicates that the large N limit leads to the same free energy as the high-temperature limit.

Similarly, we define the free energy for H_4^{SUSY} as

$$F^{\mathrm{SUSY}}(\beta) = -\frac{1}{\beta}\log Z^{\mathrm{SUSY}}(\beta). \tag{C4}$$

In the same way as H_4, the same expressions are obtained for the free energy for H_4^{SUSY}. Fully numerical evaluations of F and F^{SUSY} are shown in Fig. 8, which are in good agreement with the above analytical evaluations. For H_4 and H_4^{SUSY}, both in the high-temperature and large N regimes, the entropy per degree of freedom is given by

$$s = -\frac{1}{N}\left(\frac{\partial F}{\partial T}\right)_N \sim \frac{1}{2}\log 2 \quad (N \to \infty). \tag{C5}$$

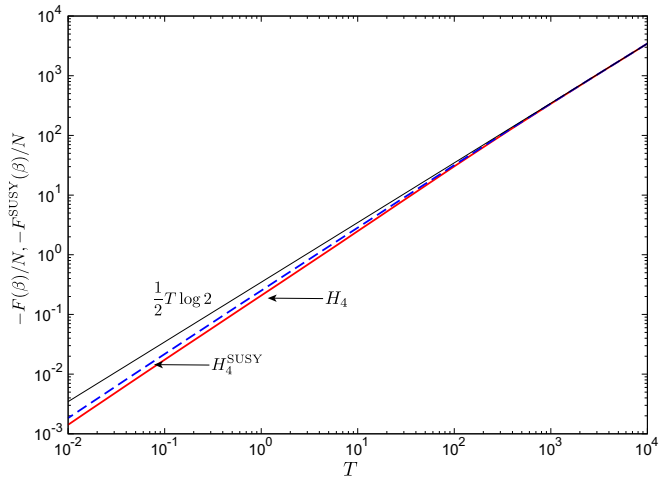

FIG. 8. Free energy per particle for H_4 (red, solid line) and H_4^{SUSY} (blue, dashed line) as functions of temperature with $N = 36$. The value at large N limit $\frac{1}{2}T\log 2$ is shown in black solid line.

APPENDIX D: DYNAMICS

In this Appendix, we derive the time evolution of γ_j in the Heisenberg picture and present detailed calculations of the dynamical correlation functions. We first note that the complex fermion operators $f_k^{\pm}$ and $g_k^{\pm}$ defined in Eqs. (A10) and (A19) satisfy

$$[H_4, f_k^{\pm}] = f_k^{\pm}\left(\pm\epsilon_k H_2 + \tfrac{1}{2}\epsilon_k^2\right), \tag{D1}$$

$$\left[H_4^{\mathrm{SUSY}}, g_k^{\pm}\right] = g_k^{\pm}\left(\pm 2\varepsilon_k H_{\mathrm{free}} + \varepsilon_k^2\right), \tag{D2}$$

where H_2 and H_{free} are defined in Eqs. (2) and (11). These commutation relations imply

$$e^{\mathrm{i}H_4 t} f_k^{\pm} e^{-\mathrm{i}H_4 t} = e^{-\frac{\mathrm{i}}{2}\epsilon_k^2 t} e^{\pm\mathrm{i}\epsilon_k H_2 t} f_k^{\pm}, \tag{D3}$$

$$e^{\mathrm{i}H_4^{\mathrm{SUSY}} t} g_k^{\pm} e^{-\mathrm{i}H_4^{\mathrm{SUSY}} t} = e^{-\mathrm{i}\varepsilon_k^2 t} e^{\pm 2\mathrm{i}\varepsilon_k H_{\mathrm{free}} t} g_k^{\pm}. \tag{D4}$$

Since the Majorana and complex fermion operators are related by the Fourier transform

$$\begin{aligned} f_k^{\pm} &= \frac{1}{2}(\psi_{2k-1} \mp \mathrm{i}\psi_{2k}) \\ &= \sqrt{\frac{1}{2N}}\sum_{j=1}^{N} e^{\mp\mathrm{i}(j-1)\theta_k}\gamma_j, \quad \left(1 \leqslant k \leqslant \frac{N}{2}\right), \end{aligned} \tag{D5}$$

$$\begin{aligned} g_k^{\pm} &= \frac{1}{2}(\chi_{2k-1} \mp \mathrm{i}\chi_{2k}) \\ &= \sqrt{\frac{1}{2N}}\sum_{j=1}^{N} e^{\mp\mathrm{i}(j-1)\vartheta_k}\gamma_j \quad \left(1 \leqslant k \leqslant \frac{N}{2} - 1\right), \end{aligned} \tag{D6}$$

γ_j can be expressed in terms of the complex fermion operators as

$$\gamma_j = \sqrt{\frac{2}{N}}\sum_{s=\pm}\sum_{k=1}^{N/2} e^{\mathrm{i}s(j-1)\theta_k} f_k^{\pm} \tag{D7}$$

for H_4 and

$$\gamma_j = \frac{1}{\sqrt{N}}\chi_0 + \frac{(-1)^{j-1}}{\sqrt{N}}\chi_{N/2} + \sqrt{\frac{2}{N}}\sum_{s=\pm}\sum_{k=1}^{\frac{N}{2}-1} e^{\mathrm{i}s(j-1)\vartheta_k} g_k^{\pm} \tag{D8}$$

for H_4^{SUSY}. Combining Eqs. (D3), (D4), (D7), and (D8), we obtain the time evolution of γ_j as

$$\gamma_j(t) := e^{\mathrm{i}H_4 t}\gamma_j e^{-\mathrm{i}H_4 t} = \sqrt{\frac{2}{N}}\sum_{s=\pm}\sum_{k=1}^{\frac{N}{2}} e^{\mathrm{i}s(j-1)\theta_k} e^{-\frac{\mathrm{i}}{2}\epsilon_k^2 t} e^{\mathrm{i}s\epsilon_k H_2 t} f_k^s, \tag{D9}$$

$$\tilde{\gamma}_j(t) := e^{\mathrm{i}H_4^{\mathrm{SUSY}} t}\gamma_j e^{-\mathrm{i}H_4^{\mathrm{SUSY}} t} = \frac{1}{\sqrt{N}}\chi_0 + \frac{(-1)^{j-1}}{\sqrt{N}}\chi_{N/2} + \sqrt{\frac{2}{N}}\sum_{s=\pm}\sum_{k=1}^{\frac{N}{2}-1} e^{\mathrm{i}s(j-1)\vartheta_k} e^{-\mathrm{i}\varepsilon_k^2 t} e^{2\mathrm{i}s\varepsilon_k H_{\mathrm{free}} t} g_k^s. \tag{D10}$$

1. Autocorrelation functions

We first consider the autocorrelation functions for H_4, which is obtained by setting $l = m$ in Eq. (24),

$$G_{ll}(t,\beta) = \mathrm{Tr}[\rho\gamma_l(t)\gamma_l(0)], \tag{D11}$$

where $\rho = \exp(-\beta H_4)/\mathrm{Tr}\exp(-\beta H_4)$. Substituting Eq. (D9) to Eq. (D11), we obtain

$$G_{ll}(t) = \frac{2}{NZ(\beta)}\mathrm{Tr}\left[e^{-\frac{\beta}{2}(H_2)^2-\beta E_0}\sum_{k=1}^{N/2} e^{-\frac{\mathrm{i}}{2}\epsilon_k^2 t} e^{\mathrm{i}\epsilon_k H_2 t\sigma_k}\right] \tag{D12}$$

$$= \frac{2}{Nz(\beta)}\sum_{k=1}^{N/2}\int_{-\infty}^{\infty} dx e^{-\frac{2}{\beta}x^2} e^{\mathrm{i}x\epsilon_k}\prod_{k'\neq k}\cos\left(\frac{\epsilon_k\epsilon_{k'}t}{2} + x\epsilon_{k'}\right), \tag{D13}$$

with $\sigma_k = 2n_k - 1$ and we have used the HS transformation.

For H_4^{SUSY}, the two-point function is similarly defined as

$$G_{lm}^{\mathrm{SUSY}}(t) := \mathrm{Tr}[\rho\tilde{\gamma}_l(t)\tilde{\gamma}_m(0)], \tag{D14}$$

where $\rho = \exp(-\beta H_4^{\mathrm{SUSY}})/\mathrm{Tr}\exp(-\beta H_4^{\mathrm{SUSY}})$. We now evaluate the autocorrelation function $G_{ll}^{\mathrm{SUSY}}(t)$. Substituting Eq. (D10) to Eq. (D14), we obtain

$$G_{ll}^{\mathrm{SUSY}}(t) = \frac{2}{N} + \frac{2}{Nz^{\mathrm{SUSY}}(\beta)}\sum_{k=1}^{N/2-1}\int_{-\infty}^{\infty} dx e^{-\frac{x^2}{\beta}} e^{\mathrm{i}x\varepsilon_k} \times \prod_{k'\neq k}\cos(\varepsilon_k\varepsilon_{k'}t + x\varepsilon_{k'}), \tag{D15}$$

where the first constant term originates from the Majorana zero modes contained in Eq. (D10).

By numerical integration, we evaluate Eqs. (D13) and (D15) as functions of time for several β. The results are presented in Figs. 3(a) and 3(b), respectively. We note that exponential decay of $|G_{ll}^{\mathrm{SUSY}}(t) - \frac{2}{N}|$ shown in Fig. 3(b) implies the residual value $\frac{2}{N}$.

2. Out-of-time-order correlators

a. Clean SYK model

Next, we compute the OTOC for H_4. Substituting $\gamma_j(t)$ [Eq. (D9)] for Eq. (26) and using the commutation relation Eq. (D1), we perform the sum over l and m, and obtain

$$F(t,\beta) = -\frac{4}{N^2}\sum_{k_1\neq k_2} e^{-\frac{\beta}{4}(\epsilon_{k_1}^2+\epsilon_{k_2}^2)} \times \mathrm{Tr}\left[\rho e^{\frac{\beta}{2}(\sigma_{k_1}\epsilon_{k_1}+\sigma_{k_2}\epsilon_{k_2})H_2} e^{(\mathrm{i}t-\frac{\beta}{4})\sigma_{k_1}\sigma_{k_2}\epsilon_{k_1}\epsilon_{k_2}}\right]. \tag{D16}$$

First, we consider the case with $\beta = 0$. In this case, we have

$$F(t,0) = -\frac{4}{N^2}\sum_{k_1,k_2}\cos(\epsilon_{k_1}\epsilon_{k_2}t) + \frac{4}{N^2}\sum_{k_1}\cos\left(\epsilon_{k_1}^2 t\right). \tag{D17}$$

The first term can be computed analytically in the large-N limit:

$$\begin{aligned} -\frac{4}{N^2}\sum_{k_1,k_2}\cos(\epsilon_{k_1}\epsilon_{k_2}t) &\simeq -\frac{1}{\pi^2}\int_0^{\infty} d\epsilon_1\int_0^{\infty} d\epsilon_2\cos(\epsilon_1\epsilon_2 t) \times \frac{1}{1+\left(\frac{\epsilon_1}{2}\right)^2}\frac{1}{1+\left(\frac{\epsilon_2}{2}\right)^2} \\ &= -\frac{2}{\pi}(\sin 4t\,\mathrm{Ci}\,4t - \cos 4t\,\mathrm{si}\,4t) \\ &= -\frac{2}{\pi}f(4t), \end{aligned} \tag{D18}$$

where $\mathrm{si}\,x$ and $\mathrm{Ci}\,x$ are sine and cosine integrals defined by

$$\mathrm{si}\,x = -\int_x^{\infty}\frac{\sin t}{t}dt \quad\text{and}\quad \mathrm{Ci}\,x = -\int_x^{\infty}\frac{\cos t}{t}dt, \tag{D19}$$

and

$$f(t) := \sin t\,\mathrm{Ci}\,t - \cos t\,\mathrm{si}\,t = \int_0^{\infty}\frac{\sin u}{u+t}du \tag{D20}$$

is one of the auxiliary functions for the trigonometric integrals [57]. We now evaluate the second term in Eq. (D17). The estimate reads

$$\left|\frac{4}{N^2}\sum_{k_1=1}^{N/2}\cos\left(\epsilon_{k_1}^2 t\right)\right| \simeq \frac{2}{N}\left|\int_0^{\infty}\frac{1}{\pi}\frac{\cos(\epsilon^2 t)}{1+\left(\frac{\epsilon}{2}\right)^2}d\epsilon\right| \leqslant \frac{2}{N}\int_0^{\infty}\frac{1}{\pi}\frac{1}{1+\left(\frac{\epsilon}{2}\right)^2}d\epsilon = \frac{2}{N}, \tag{D21}$$

which means that this term is negligible in the large-N limit. Thus, we conclude that Eq. (D18) dominates the behavior of $F(t,0)$. Furthermore, we obtain the asymptotic form

$$F(t,0) = -\frac{1}{2\pi t} + O\left(t^{-2}, \frac{1}{N}\right). \tag{D22}$$

Next, we consider the finite-temperature OTOC. By the HS transformation,

$$e^{-\frac{\beta}{2}A^2} = \sqrt{\frac{\beta}{2\pi}}\int dx e^{-\frac{\beta}{2}x^2} e^{\mathrm{i}x\beta A}, \tag{D23}$$

TABLE III. Fitting parameters for OTOC for H_4.

β	A	$\lambda'(=\beta\lambda)$	B	a_0	a_1	a_2
2.0	0.02051	3.791	−0.2058	−0.1844	0.05887	0.2631
1.0	0.01751	4.342	−0.2933	−0.2745	0.05444	0.3203
0.5	0.01339	4.801	−0.3936	−0.3788	0.03659	0.3208
0.2	0.008131	5.247	−0.5311	−0.5218	0.01969	0.2491
0.1	0.005102	5.483	−0.6281	−0.6221	0.01111	0.1768
0.05	0.003011	5.652	−0.7124	−0.7088	0.005931	0.1138

with $A = H_2 - \frac{1}{2}(\sigma_{k_1}\epsilon_{k_1} + \sigma_{k_2}\epsilon_{k_2})$, we obtain the OTOC in the integral form as

$$F(t,\beta) = -\frac{4}{z(\beta)N^2}\sum_{k_1\neq k_2} e^{-\frac{\beta}{8}(\epsilon_{k_1}^2+\epsilon_{k_2}^2)}\cos\left(\epsilon_{k_1}\epsilon_{k_2}t\right) \times \int_{-\infty}^{\infty} dx e^{-\frac{2x^2}{\beta}} \prod_{k'\in K\setminus\{k_1,k_2\}} \cos(x\epsilon_{k'}),$$

where $K = \{1, 2, \ldots, \frac{N}{2}\}$. This formulation enables us to evaluate $F(t,\beta)$ for large N, and the result is shown in Fig. 4(a) in the main text.

Here, we provide details of the fitting of the OTOC. We perform the fitting using exponential and polynomial functions in the interval $[0.1\beta, 0.2\beta]$,

$$f_1(t) = Ae^{\lambda' t/\beta} + B, \tag{D24}$$

$$f_2(t) = a_0 + a_1\left(\frac{t}{\beta}\right) + a_2\left(\frac{t}{\beta}\right)^2, \tag{D25}$$

where A, $\lambda'(=\lambda\beta)$, B, a_0, a_1, and a_2 are the fitting parameters. The results for H_4 are shown in Table III and Fig. 9. We find that the exponential fit is better because a simple proportional relation between the fitted exponent and temperature is found, which is predicted for quantum many-body chaotic systems. However, for the polynomial fit, we find no simple relation between the fitted parameters and temperature.

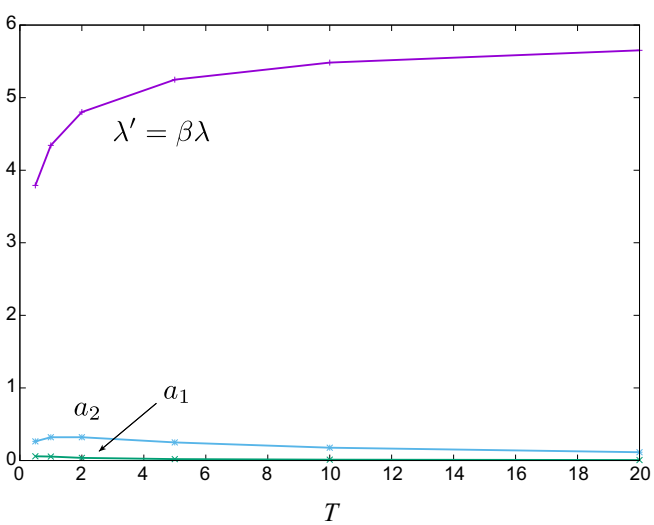

FIG. 9. Fitting parameters as functions of the temperature T.

TABLE IV. Fitting parameters for OTOC for H_4^{SUSY}.

β	A	$\lambda'(=\beta\lambda)$	B
0.5	0.01774	4.354	−0.2953
0.2	0.01199	4.937	−0.4298
0.1	0.008119	5.258	−0.5342
0.05	0.005122	5.479	−0.6315

b. Clean SUSY SYK model

Similar to H_4, we can calculate the OTOC for the clean SUSY SYK model. We obtain the finite-temperature OTOC for $H_4{}^{\mathrm{SUSY}}$ as

$$\begin{aligned} F^{\mathrm{SUSY}}(t,\beta) &= \frac{1}{N^2}\sum_{l,m=1}^{N/2}\mathrm{Tr}\left[\rho^{\frac{1}{4}}\tilde{\gamma}_l(t)\rho^{\frac{1}{4}}\tilde{\gamma}_m(0)\rho^{\frac{1}{4}}\tilde{\gamma}_l(t)\rho^{\frac{1}{4}}\tilde{\gamma}_m(0)\right] \\ &= -\frac{4}{N^2}\sum_{k_1\neq k_2} e^{-\frac{\beta}{2}(\varepsilon_{k_1}^2+\varepsilon_{k_2}^2)} \\ &\quad\times \mathrm{Tr}\left[\rho e^{\beta(\sigma_{k_1}\varepsilon_{k_1}+\sigma_{k_2}\varepsilon_{k_2})H_{\mathrm{free}}} e^{(2it-\frac{\beta}{2})\sigma_{k_1}\sigma_{k_2}\varepsilon_{k_1}\varepsilon_{k_2}}\right] \\ &\quad -\frac{8}{N^2}\sum_{k_1=1}^{\frac{N}{2}-1}\mathrm{Tr}\left[\rho e^{-\frac{\beta}{2}(\varepsilon_{k_1}^2-2\sigma_{k_1}\varepsilon_{k_1}H_{\mathrm{free}})}\right]. \end{aligned} \tag{D26}$$

As done for the OTOC of H_4 at $\beta = 0$, we obtain

$$\begin{aligned} F^{\mathrm{SUSY}}(t,0) &= -\frac{4}{N^2}\sum_{k_1,k_2}\left[\cos(2\varepsilon_{k_1}\varepsilon_{k_2}t) - \delta_{k_1,k_2}\cos\left(2\varepsilon_{k_1}^2 t\right)\right] \\ &\quad -\frac{4(N-2)}{N^2} \\ &\simeq -\frac{2}{\pi}(\sin 8t\,\mathrm{Ci}\,8t - \cos 8t\,\mathrm{si}\,8t) + O\left(\frac{1}{N}\right) \\ &= -\frac{1}{4\pi t} + O\left(t^{-2}, \frac{1}{N}\right). \end{aligned} \tag{D27}$$

Using the HS transformation, we obtain the OTOC for H_4^{SUSY} at finite temperature in the integral form as

$$\begin{aligned} F^{\mathrm{SUSY}}(t,\beta) &= -\frac{4}{z^{\mathrm{SUSY}}(\beta)N^2}\sum_{k_1\neq k_2} e^{-\frac{\beta}{4}(\varepsilon_{k_1}^2+\varepsilon_{k_2}^2)}\cos\left(2\varepsilon_{k_1}\varepsilon_{k_2}t\right) \\ &\quad\times\int_{-\infty}^{\infty} dx e^{-\frac{x^2}{\beta}} \prod_{k'\in K^{\mathrm{SUSY}}\setminus\{k_1,k_2\}}\cos(x\varepsilon_{k'}) \\ &\quad -\frac{8}{z^{\mathrm{SUSY}}(\beta)N^2}\sum_{k_1} e^{-\frac{\beta}{4}\varepsilon_{k_1}^2}\int_{-\infty}^{\infty} dx e^{-\frac{x^2}{\beta}} \\ &\quad\times\prod_{k'\in K^{\mathrm{SUSY}}\setminus\{k_1\}}\cos(x\varepsilon_{k'}), \end{aligned} \tag{D28}$$

with $K^{\mathrm{SUSY}} = \{1, \ldots, \frac{N}{2} - 1\}$. The numerical evaluation of $F^{\mathrm{SUSY}}(t,\beta)$ is shown in Fig. 4(b) and the results of exponential fitting are summarized in Table IV, which are quite similar to those of $F(t,\beta)$ for H_4.

c. Quadratic clean SYK model H_2

To see the fact that the scrambling behavior of the OTOC is characteristic in four-body SYK-like systems, we calculate the OTOC for H_2 at the infinite temperature. The OTOC for H_2 is obtained as

$$F_{\text{quad}}(t) = \frac{1}{N^2}\sum_{l,m} 2^{-\frac{N}{2}}\text{Tr}[\bar{\gamma}_l(t)\bar{\gamma}_m(0)\bar{\gamma}_l(t)\bar{\gamma}_m(0)] = -1 + \frac{2}{N}, \tag{D29}$$

with $\bar{\gamma}_l(t) = e^{\mathrm{i}H_2 t}\gamma_l e^{-\mathrm{i}H_2 t}$, which does not depend on time.

d. Free fermion chain

As another example of a noninteracting system, we consider the OTOC for a free-fermion chain. The Hamiltonian is given by

$$H_{1\text{d}} = -\sum_{i=1}^{N} c_i^\dagger c_{i+1} + \text{H.c.}, \tag{D30}$$

where c_i ($c_i^\dagger$) is an annihilation (creation) operator for fermion at site i, we have set the hopping integral to be unity, and periodic boundary conditions are imposed: $c_{N+1} = c_1$ and $c_{N+1}^\dagger = c_1^\dagger$. We define the OTOC for this complex fermion system in a manner similar to that described in Ref. [58], as

$$F_{1\text{d}}(t) = \frac{1}{N^2}\sum_{l,m=1}^{N} 2^{-N}\text{Tr}[c_l^\dagger(t)c_m^\dagger(0)c_l(t)c_m(0)], \tag{D31}$$

where $c_l^{(\dagger)}(t) = e^{\mathrm{i}H_{1\text{d}}t}c_l^{(\dagger)}e^{-\mathrm{i}H_{1\text{d}}t}$. Equation (D31) is calculated as

$$F_{1\text{d}}(t) = -\frac{1}{4}\left(1 - \frac{1}{N}\right), \tag{D32}$$

which does not exhibit scrambling behavior either.

[1] C. Gogolin and J. Eisert, Equilibration, thermalisation, and the emergence of statistical mechanics in closed quantum systems, Rep. Prog. Phys. **79**, 056001 (2016).

[2] J. M. Deutsch, Eigenstate thermalization hypothesis, Rep. Prog. Phys. **81**, 082001 (2018).

[3] T. Mori, T. N. Ikeda, E. Kaminishi, and M. Ueda, Thermalization and prethermalization in isolated quantum systems: A theoretical overview, J. Phys. B: At. Mol. Opt. Phys. **51**, 112001 (2018).

[4] L. D'Alessio, Y. Kafri, A. Polkovnikov, and M. Rigol, From quantum chaos and eigenstate thermalization to statistical mechanics and thermodynamics, Adv. Phys. **65**, 239 (2016).

[5] F. Borgonovi, F. M. Izrailev, L. F. Santos, and V. G. Zelevinsky, Quantum chaos and thermalization in isolated systems of interacting particles, Phys. Rep. **626**, 1 (2016).

[6] H. Liu and J. Sonner, Quantum many-body physics from a gravitational lens, Nat. Rev. Phys. **2**, 615 (2020).

[7] M. Serbyn, D. A. Abanin, and Z. Papić, Quantum many-body scars and weak breaking of ergodicity, Nat. Phys. **17**, 675 (2021).

[8] S. Moudgalya, N. Regnault, and B. A. Bernevig, Quantum many-body scars and Hilbert space fragmentation: A review of exact results, Rep. Prog. Phys. **85**, 086501 (2022).

[9] A. Chandran, T. Iadecola, V. Khemani, and R. Moessner, Quantum many-body scars: A quasiparticle perspective, Annu. Rev. Condens. Matter Phys. **14**, 443 (2023).

[10] R. Nandkishore and D. A. Huse, Many-body localization and thermalization in quantum statistical mechanics, Annu. Rev. Condens. Matter Phys. **6**, 15 (2015).

[11] F. Alet and N. Laflorencie, Many-body localization: An introduction and selected topics, C. R. Phys. **19**, 498 (2018).

[12] D. A. Abanin, E. Altman, I. Bloch, and M. Serbyn, Colloquium: Many-body localization, thermalization, and entanglement, Rev. Mod. Phys. **91**, 021001 (2019).

[13] P. Hayden and J. Preskill, Black holes as mirrors: Quantum information in random subsystems, J. High Energy Phys. 09 (2007) 120.

[14] Y. Sekino and L. Susskind, Fast scramblers, J. High Energy Phys. 10 (2008) 065.

[15] S. H. Shenker and D. Stanford, Black holes and the butterfly effect, J. High Energy Phys. 03 (2014) 067.

[16] S. H. Shenker and D. Stanford, Stringy effects in scrambling, J. High Energy Phys. 05 (2015) 132.

[17] J. Maldacena, S. H. Shenker, and D. Stanford, A bound on chaos, J. High Energy Phys. 08 (2016) 106.

[18] S. Sachdev and J. Ye, Gapless spin-fluid ground state in a random quantum Heisenberg magnet, Phys. Rev. Lett. **70**, 3339 (1993).

[19] A. Kitaev, A Simple Model of Quantum Holography, KITP Program: Entanglement in Strongly-Correlated Quantum Matter (Santa Barbara, 2015), https://online.kitp.ucsb.edu/online/entangled15/kitaev/.

[20] D. A. Trunin, Pedagogical introduction to the Sachdev–Ye–Kitaev model and two-dimensional dilaton gravity, Phys. Usp. **64**, 219 (2021).

[21] V. Rosenhaus, An introduction to the SYK model, J. Phys. A: Math. Theor. **52**, 323001 (2019).

[22] D. Chowdhury, A. Georges, O. Parcollet, and S. Sachdev, Sachdev-Ye-Kitaev models and beyond: Window into non-Fermi liquids, Rev. Mod. Phys. **94**, 035004 (2022).

[23] J. Kudler-Flam, L. Nie, and S. Ryu, Conformal field theory and the web of quantum chaos diagnostics, J. High Energy Phys. 01 (2020) 175.

[24] S. W. McDonald and A. N. Kaufman, Spectrum and eigenfunctions for a Hamiltonian with stochastic trajectories, Phys. Rev. Lett. **42**, 1189 (1979).

[25] M. Berry, Quantizing a classically ergodic system: Sinai's billiard and the KKR method, Ann. Phys. **131**, 163 (1981).

[26] P. H. C. Lau, C.-T. Ma, J. Murugan, and M. Tezuka, Randomness and chaos in qubit models, Phys. Lett. B **795**, 230 (2019).

[27] E. Dyer and G. Gur-Ari, 2D CFT partition functions at late times, J. High Energy Phys. 08 (2017) 075.

[28] A. I. Larkin and Y. N. Ovchinnikov, Quasiclassical method in the theory of superconductivity, J. Exp. Theor. Phys. **28**, 1200 (1969).

[29] J. Polchinski and V. Rosenhaus, The spectrum in the Sachdev-Ye-Kitaev model, J. High Energy Phys. 04 (2016) 001.
[30] J. Maldacena and D. Stanford, Remarks on the Sachdev-Ye-Kitaev model, Phys. Rev. D **94**, 106002 (2016).
[31] N. Dowling, P. Kos, and K. Modi, Scrambling is necessary but not sufficient for chaos, Phys. Rev. Lett. **131**, 180403 (2023).
[32] E. B. Rozenbaum, S. Ganeshan, and V. Galitski, Lyapunov exponent and out-of-time-ordered correlator's growth rate in a chaotic system, Phys. Rev. Lett. **118**, 086801 (2017).
[33] E. B. Rozenbaum, S. Ganeshan, and V. Galitski, Universal level statistics of the out-of-time-ordered operator, Phys. Rev. B **100**, 035112 (2019).
[34] K. Hashimoto, K.-B. Huh, K.-Y. Kim, and R. Watanabe, Exponential growth of out-of-time-order correlator without chaos: Inverted harmonic oscillator, J. High Energy Phys. 11 (2020) 068.
[35] T. Akutagawa, K. Hashimoto, T. Sasaki, and R. Watanabe, Out-of-time-order correlator in coupled harmonic oscillators, J. High Energy Phys. 08 (2020) 013.
[36] T. Xu, T. Scaffidi, and X. Cao, Does scrambling equal chaos? Phys. Rev. Lett. **124**, 140602 (2020).
[37] Y.-Z. You, A. W. W. Ludwig, and C. Xu, Sachdev-Ye-Kitaev model and thermalization on the boundary of many-body localized fermionic symmetry-protected topological states, Phys. Rev. B **95**, 115150 (2017).
[38] A. M. García-García and J. J. M. Verbaarschot, Spectral and thermodynamic properties of the Sachdev-Ye-Kitaev model, Phys. Rev. D **94**, 126010 (2016).
[39] J. S. Cotler, G. Gur-Ari, M. Hanada, J. Polchinski, P. Saad, S. H. Shenker, D. Stanford, A. Streicher, and M. Tezuka, Black holes and random matrices, J. High Energy Phys. 05 (2017) 118.
[40] A. M. García-García, B. Loureiro, A. Romero-Bermúdez, and M. Tezuka, Chaotic-integrable transition in the Sachdev-Ye-Kitaev model, Phys. Rev. Lett. **120**, 241603 (2018).
[41] A. Kitaev and S. J. Suh, The soft mode in the Sachdev-Ye-Kitaev model and its gravity dual, J. High Energy Phys. 05 (2018) 183.
[42] See Refs. [58–63] for other disorder-free variants of the SYK models.
[43] P. H. C. Lau, C.-T. Ma, J. Murugan, and M. Tezuka, Correlated disorder in the SYK_2 model, J. Phys. A: Math. Theor. **54**, 095401 (2021).
[44] W. Fu, D. Gaiotto, J. Maldacena, and S. Sachdev, Supersymmetric Sachdev-Ye-Kitaev models, Phys. Rev. D **95**, 026009 (2017).
[45] E. Jaynes and F. Cummings, Comparison of quantum and semiclassical radiation theories with application to the beam maser, Proc. IEEE **51**, 89 (1963).
[46] Y. Hatsugai and M. Kohmoto, Exactly solvable model of correlated lattice electrons in any dimensions, J. Phys. Soc. Jpn. **61**, 2056 (1992).
[47] S. He, P. H. C. Lau, Z.-Y. Xian, and L. Zhao, Quantum chaos, scrambling and operator growth in $T\overline{T}$ deformed SYK models, J. High Energy Phys. 12 (2022) 070.
[48] F. Haake, *Quantum Signatures of Chaos* (Springer, Berlin, 2010).
[49] A. M. García-García and M. Tezuka, Many-body localization in a finite-range Sachdev-Ye-Kitaev model and holography, Phys. Rev. B **99**, 054202 (2019).
[50] T. Guhr, A. Müller–Groeling, and H. A. Weidenmüller, Random-matrix theories in quantum physics: Common concepts, Phys. Rep. **299**, 189 (1998).
[51] S. Ozaki and H. Nakazato, Analytic approach to dynamics of the resonant and off-resonant Jaynes-Cummings systems with cavity losses, Phys. Rev. A **103**, 053713 (2021).
[52] I. Kukuljan, S. Grozdanov, and T. Prosen, Weak quantum chaos, Phys. Rev. B **96**, 060301(R) (2017).
[53] R. Prakash and A. Lakshminarayan, Scrambling in strongly chaotic weakly coupled bipartite systems: Universality beyond the Ehrenfest timescale, Phys. Rev. B **101**, 121108(R) (2020).
[54] C.-J. Lin and O. I. Motrunich, Out-of-time-ordered correlators in a quantum Ising chain, Phys. Rev. B **97**, 144304 (2018).
[55] J.-H. Bao and C.-Y. Zhang, Out-of-time-order correlators in the one-dimensional XY model, Commun. Theor. Phys. **72**, 085103 (2020).
[56] B. Kobrin, Z. Yang, G. D. Kahanamoku-Meyer, C. T. Olund, J. E. Moore, D. Stanford, and N. Y. Yao, Many-body chaos in the Sachdev-Ye-Kitaev model, Phys. Rev. Lett. **126**, 030602 (2021).
[57] NIST Digital Library of Mathematical Functions, https://dlmf.nist.gov/.
[58] E. Iyoda, H. Katsura, and T. Sagawa, Effective dimension, level statistics, and integrability of Sachdev-Ye-Kitaev-like models, Phys. Rev. D **98**, 086020 (2018).
[59] E. Witten, An SYK-like model without disorder, J. Phys. A: Math. Theor. **52**, 474002 (2019).
[60] I. R. Klebanov and G. Tarnopolsky, Uncolored random tensors, melon diagrams, and the Sachdev-Ye-Kitaev models, Phys. Rev. D **95**, 046004 (2017).
[61] C. Krishnan, K. Pavan Kumar, and D. Rosa, Contrasting SYK-like models, J. High Energy Phys. 01 (2018) 064.
[62] V. Balasubramanian, M. DeCross, A. Kar, Y. C. Li, and O. Parrikar, Complexity growth in integrable and chaotic models, J. High Energy Phys. 07 (2021) 011.
[63] B. Craps, M. D. Clerck, O. Evnin, P. Hacker, and M. Pavlov, Bounds on quantum evolution complexity via lattice cryptography, SciPost Phys. **13**, 090 (2022).